Analysing the potential of UAV point cloud as input in quantitative structure modelling for assessment of woody biomass of windbreaks and single trees

NING YE
February 2018

SUPERVISORS:
ir. L.M. van Leeuwen
dr. Panagiotis Nyktas

Analysing the potential of UAV point cloud as input in quantitative structure modelling for assessment of woody biomass of windbreaks and single trees

NING YE
Enschede, The Netherlands, February 2018

Thesis submitted to the Faculty of Geo-Information Science and Earth Observation of the University of Twente in partial fulfilment of the requirements for the degree of Master of Science in Geo-information Science and Earth Observation.
Specialization: Natural Resources Management

SUPERVISORS:
ir. L.M. van Leeuwen (1st supervisor)
dr. Panagiotis Nyktas (2nd supervisor)

THESIS ASSESSMENT BOARD:
dr. Y.A. Hussin (Chair)
dr. Tuomo Kauranne (External Examiner, Lappeenranta University of Technology - Finland)

ABSTRACT

Accurate tree metrics is essential for forest management. Quantitative Structure Model (QSM) which can reconstruct an accurate 3D model of trees, has been used with Terrestrial Laser Scanning (TLS) point cloud as input. However, image-based Structure from Motion (SfM) can produce point cloud as well. Unmanned Aerial Vehicle (UAV), which can collect images of a large scale in a short period, seems like a good choice for forest study.

This study aims to investigate the feasibility of UAV point cloud for QSM of windbreaks. Flights were carried out during the leaf-on and leaf-off seasons with an inclined camera onboard. Four oblique camera angles were used during the leaf-on season to obtain the optimal angle for UAV data collection. The Diameter at Breast Height (DBH) and height derived from UAV point cloud and QSM, also the DBH estimated by Canopy Projection Area (CPA), were compared with field measured data. The biomass calculated through allometry was compared with the QSM-based biomass. The accuracy of biomass estimations was assessed with reference, which was calculated using field measured DBH and height through the allometry.

In this study, the point density increased with the increase of oblique camera angle. DBH extracted from the UAV-generated point cloud, DBH estimated by CPAs versus reference showed no significant difference ($p>0.05$), while a significant difference was found between QSM-estimated DBH and the reference DBH. No significant difference was seen only between height extracted from the point cloud and the field-measured height for the leaf-on season. Significant differences existed between estimated height and ALS-extracted height for the leaf-on and leaf-off seasons both. The QSM-based biomass showed 45.88% underestimation for the leaf-on season and 43.26% underestimation for the leaf-off season.

The study shows the potential of UAV point cloud for QSM reconstruction. Besides, the density of UAV point cloud increases with the increase of oblique camera angle, but the lower angle is better for feature point detection. For the further work, the flight condition should be considered, and the flight should be well planned beforehand. The data collection is better carried out during the leaf-off season without foliage occlusion problem.

ACKNOWLEDGEMENTS

I would first like to thank ir. Louise van Leeuwen for her continuous support of my thesis, for her patience, motivation, valuable suggestions. Secondly, I would like to thank dr. Panagiotis Nyktas, for the kind help during my work. Thanks to my parents for the unconditional love, I miss you so much. Finally, I would like to thank everyone who supported and encouraged me throughout the 6-month suffering. Cheers!

Ning Ye

Enschede, January 2018

TABLE OF CONTENTS

LIST OF FIGURES

LIST OF TABLES

1. INTRODUCTION

1.1. Background

Windbreaks, also named shelterbelts, are trees planted in a linear shape across crop/grazing areas or along roads, and they usually consist of one or more rows of trees or shrubs (Udawatta & Jose, 2012). Except for the functions of microclimate modification and crop protection, windbreaks planted in an agricultural area can provide food and habitat for wildlife and livestock. Economic and farm products can also be harvested from specific windbreak trees. The shelterbelts planted along the roads have the capability of reducing noise and dust caused by vehicles, as well as improving scenic beauty.

Windbreaks play a more important role in carbon storage than general crops. This is mainly because most of the carbon stored in agricultural plants would be released back to the atmosphere by seasonal harvesting, while trees that are introduced into the agricultural system as windbreak will be retained for a longer period (Schoeneberger, 2009). Moreover, the forest products produced by the windbreak can also be used for furniture and handicraft production. As a result, carbon stored in the form of windbreaks would not be easily and quickly emitted as greenhouse gases.

Because of the considerable benefits, there is an increasing application of trees in windbreaks. Consequently, trees and shrubs, which have better abilities for biomass production and carbon sequestration than general field crops, are increasingly introduced in agricultural systems and cityscapes (Kirby & Potvin, 2007).

However, there are fewer studies about the biomass and carbon estimation of windbreaks compared with those of general forests. The lack of standard methods and procedures makes windbreak biomass estimation challenging since most biomass equations for wood are developed based on forest stands (Nair, Kumar, & Nair, 2009). The windbreaks that belong to the agroforest system have less competition, and larger amounts of available nutrients will lead to an underestimation when using general biomass equations. Meanwhile, the allometry is usually developed based on Diameter at Breast Height (DBH) and height which are strongly correlated to the biomass. Efficient and accurate method for measuring DBH and tree height is highly needed.

There are many related studies about forest biomass estimation. Invasive methods, such as felling and weighing, are commonly used for the exact measurement of biomass, which can be expensive, time-consuming and not feasible for all conditions (Dittmann, Thiessen, & Hartung, 2017). Therefore, non-invasive methods are increasingly used for biomass measurement, for instance, applications of remote sensing. However, the accuracies of these methods are not as high as the invasive methods. Hence, it is essential to find a non-invasive biomass estimation method that can appropriately balance the relationship between accuracy and efficiency. The study of Dittmann et al. (2017) shows the performances of non-invasive methods: he indicates that Lidar and Unmanned Aerial Vehicle (UAV) data, combined with allometry, are the most efficient and most accurate methods for biomass estimation of a single tree and small scale; while allometric approaches and optical images are limited by accuracy, scale, and the cost of time.

As one of the most efficient and accurate non-invasive methods for biomass calculation in forests, Structure from Motion (SfM) based on UAV data has been progressively used for detecting forest attributes. UAVs are used as aircrafts, which can acquire high-resolution images, even with an ordinary camera, by flying at low altitudes (Mader, Blaskow, Westfeld, & Maas, 2015). Because the UAV flight height is usually low, UAV based remote sensing is rarely affected by clouds and the flight plan can be more flexible and easily manipulated

(Rango, Laliberte, & Havstad, 2014). After UAV data acquisition, the acquired data can be used for SfM to obtain the required products: point cloud and orthophoto.
SfM is a photogrammetric range image technique, and it has the capability of providing exact 3D point clouds from a sequence of 2D images acquired by efficient and lightweight instruments (Figure 1).

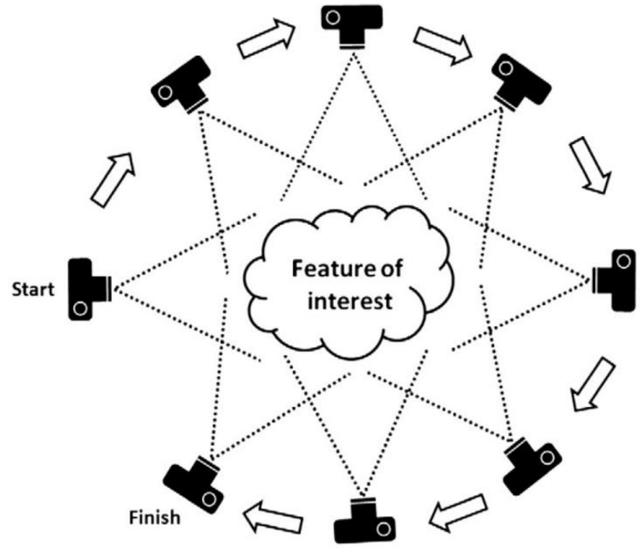

Figure 1. Image collection for SfM (Westoby, Brasington, Glasser, Hambrey, & Reynolds, 2012). Multiple and overlapping images for feature detection and scene reconstruction by SfM.

The steps of SfM are briefly described by Pollefeys et al. (2004). First, feature points are detected, and the corresponding feature points are found in multiple images; then, the matching feature points are used for image matching (Figure 2).

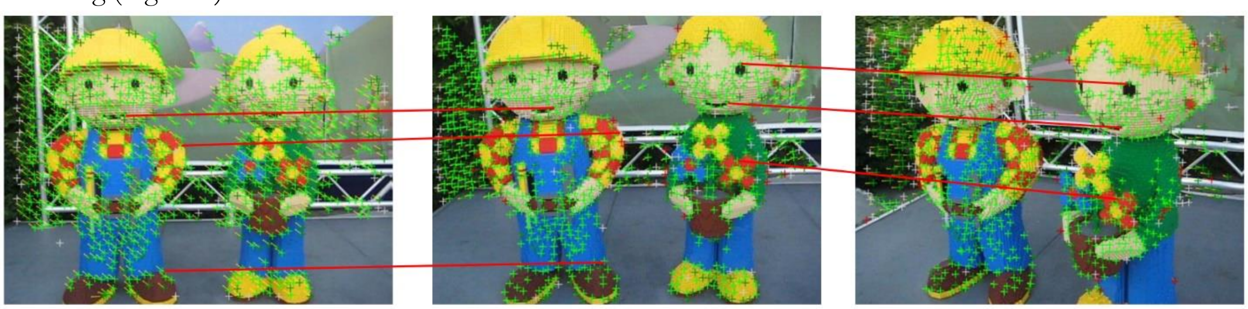

Figure 2. Feature detection by SfM (Nex, 2017). The three images are taken at different positions of same objects. The green points are the detected feature points; the red lines are examples of matching feature points.

Second, corresponding feature points from 2 adjacent images are used to estimate the motion and structure of the camera, which are also known as extrinsic parameters and intrinsic parameters, respectively, and to reconstruct the initial structure (Figure 3). The extrinsic parameters refer to the coordinate system transformations from 3D world coordinates to 3D camera coordinates, while the intrinsic parameters include focal length, image sensor format, and the principal point of the camera (Richard Hartley, 2003).

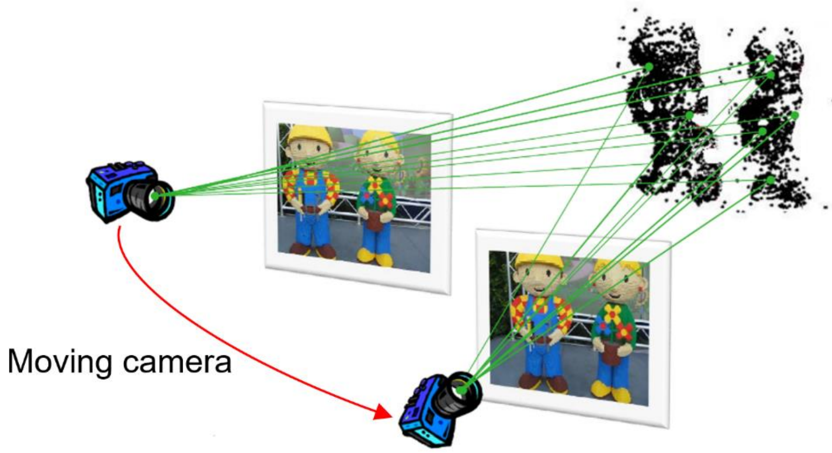

Figure 3. Initialize the structure and motion recovery in SfM (Nex, 2017). The corresponding feature points in the two images are used to recover the motion and structure of the camera, and to estimate the real-world coordinate of the feature point.

Third, for every newly added image, matches are inferred to the structure, the camera pose is calculated, and the existing structure should be refined (Figure 4). Finally, after recovering and refining the real-world structure of the features, the output will be point cloud and 3D surface, which can be used for the orthorectification process to obtain the orthophoto. As scale of the orthophoto is uniform, Crown Projection Area (CPA) of trees, which is also an important forest inventory parameter, is truly represented in the orthophoto and can be directly extracted (Bernasconi, Chirici, & Marchetti, 2017). Shah, Hussin, Leeuwen, & Gilani (2011) and Shimano (1997) studied the relationship between DBH and CPA for forest management, such as biomass estimation and modelling the forest ecosystem.

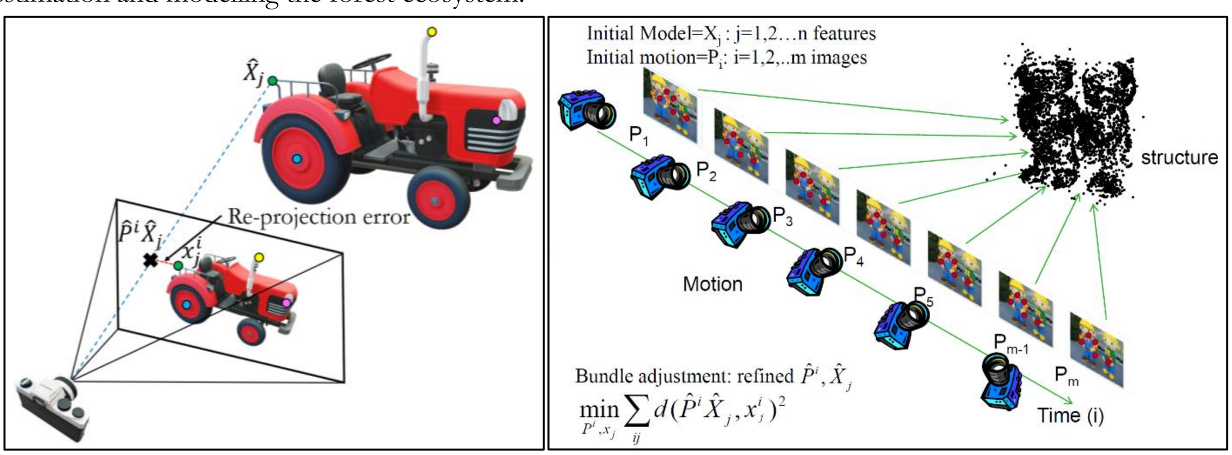

Figure 4. Refine the structure in SfM (Nex, 2017). Bundle adjustment is used to refine the structure and motion. The refinement is achieved using nonlinear least-squares algorithms to minimise the reprojection error. Here, $\boldsymbol{\hat{P}^i}$ means projection matrix, $\boldsymbol{\hat{X}_j}$ represents the 3D points, and $\boldsymbol{x_j^i}$ is the *j* point on the *i* image.

There are two main approaches for tree parameter estimation using the SfM technique: top-down approaches supported by UAV as shown in Figure 5 (Fritz, Kattenborn, & Koch, 2013; Zarco-Tejada, Diaz-Varela, Angileri, & Loudjani, 2014); and side-on approaches supported by the handheld camera as shown in Figure 6 (Miller, Morgenroth, & Gomez, 2015; Morgenroth & Gomez, 2014). The top-down method is feasible for the spatial scale of less than 5 ha, while the side-on method has only been applied to single trees, as shown in Figure 6.

Figure 5. Example of top-down approaches supported by UAV (Aicardi, Dabove, Lingua, & Piras, 2017).

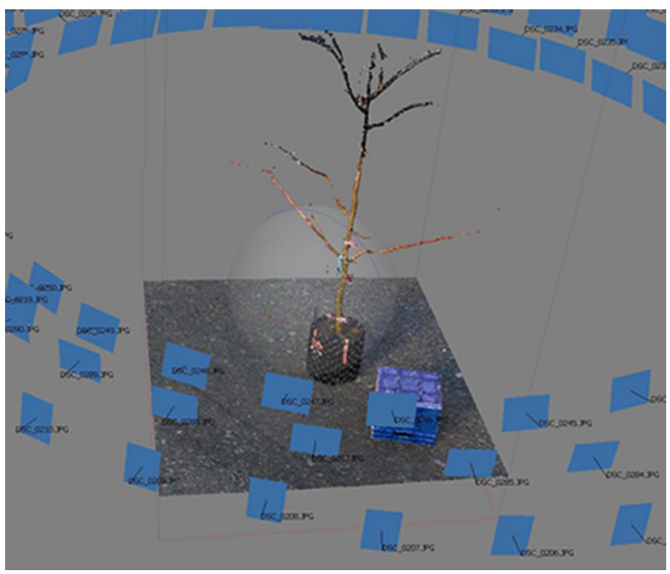

Figure 6. Example of side-on approaches supported by the handheld camera (Miller et al., 2015).

The oblique aerial image is highlighted because of its technical advantages in the remote sensing field. Compared with the traditional nadir image obtained by the top-down method, oblique imaging can record more details because the image provides a side view of the ground objects. Therefore, the identification of the hard-to-see objects, such as fine branches, can be improved; the blind spot, such as the trunk occluded by the tree crown, can be exposed (Lin, Jiang, Yao, Zhang, & Lin, 2015). The oblique image has higher efficiency than side-on approaches carried out by the handheld camera because the flight campaigns can be planned before the survey, and the UAV can fly over a large area within a short period. Hence, the use of UAV obtained oblique images seems to be a good choice for forest study.

Accurate tree metrics is crucial information for various applications, such as commercial and scientific forestry (Henning & Radtke, 2006; Næsset & Gobakken, 2008), carbon storage (Falkowski et al., 2008; Houghton, 2005; Nowak, Greenfield, Hoehn, & Lapoint, 2013) and the modeling of ecosystems (Antonarakis, Saatchi, Chazdon, & Moorcroft, 2011; Xiao & McPherson, 2011).

Quantitative Structure Modelling(QSM) is a new method for comprehensive, precise, compact, automatic and fast tree model reconstruction by using Terrestrial Laser Scanning (TLS) acquired point cloud as the input (Raumonen et al., 2013). In QSM, accurate and precise 3D models of trees can be reconstructed based on the individual tree point cloud, and branches will be represented by hierarchical collections of cylinders or other building blocks, which can be seen in Figure 7 below (Raumonen et al., 2013). Consequently, the tree parameters, such as volume and tree height, can be easily obtained for accurate biomass estimation because the direct output of QSM is the size of the cylinders. This method has been validated using volume and biomass as references through the study of Raumonen et al. (2013), Calders et al. (2013), Burt et al. (2013), and the overestimation of the retrieved Above Ground Biomass (AGB) was less than 10%, which is better than the allometric equation method with an underestimation approximately 30%.

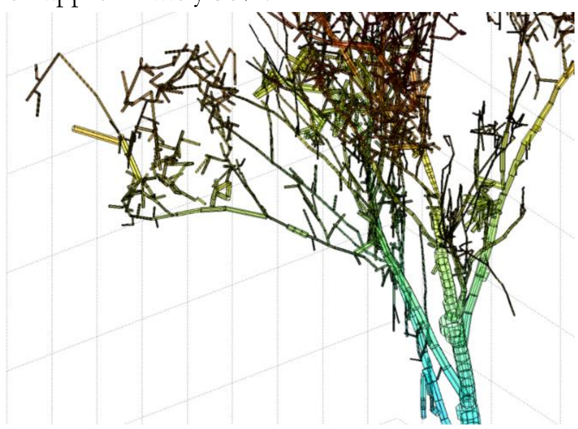

Figure 7. Example of QSM (Calders et al., 2013).

However, QSM has only been applied using TLS data. TLS is a circular-plot-based instrument, that can transmit a light pulse to objects, record the return time of the pulse and calculate the distance to the targets. Thousands of 3D points from objects can be recorded within a second by using TLS. The TLS and SfM methods can both generate point clouds, SfM models the spatial structure of objects that appear in the optical images, and the output point cloud is more like an inference, while TLS measures the spatial location of the objects. Thus, the quality of SfM point relies a lot on the image quality, while TLS is more sensitive toward the surface roughness.

1.2. Research problem

In some cases, the point cloud data generated based on UAV images could be an equally good or even better choice for the windbreak study than the TLS point cloud. TLS, which is a circular-plot-based method, would face the problem of making plots for windbreaks in a linear shape. It has been proven that an optimal cost-effective plot size of TLS is approximately 500-600 m² (the diameter of the circular plot: 25.23-27.64 m) in the work of Ruiz, Hermosilla, Mauro, & Godino (2014). The error caused by GPS overlap and co-registration is negligible within this range (Ruiz et al., 2014). Hence, at least ten plots must be sampled if the length of the windbreak is 250 m. This is inefficient. Also, when the tree lines are in swamps or some wet area, it will be difficult to enter the plot and find an appropriate location for placing the expensive TLS instruments. Besides, it is also time-consuming to move the instruments from one plot to another, while UAV just flies above the study area, and the time for image acquisition is short.

The SfM generated point cloud can be suitable for 3D tree model construction. Mader et al. (2015) compared the UAV obtained point cloud with that of TLS, and the result showed the quality of the UAV point cloud depended directly on the quality of the onboard positioning devices- the Global Positioning System (GPS) and Inertial Measurement Unit (IMU), and the accuracy and density could even be better than TLS. Fritz et al. (2013) utilised the point cloud generated by UAV images to reconstruct a 3D tree model, and results are promising.

The main problem with using the UAV point cloud for QSM is penetrating the canopy to obtain a clear view of the woody parts. The study of Raumonen et al. (2013) emphasised the necessity of a clear view for tree reconstruction, because some features of the tree, for instance, the order of magnitude of the branch, trunk size, and the approximate trunk direction, will be used to segment the trees into cylinders. Foliage occludes the branches and stems during the leaf-on season, which can result in an incorrect reconstruction. The influence caused by foliage has already been acknowledged by Raumonen et al. (2013) and Madhibha Tasiyiwa (2016), while Tilon (2017) claimed that a point cloud that included foliage could still be used for biomass estimation with an effective filtering process. However, these statements are made under the premise that the input data are TLS point clouds. For a point cloud derived from a UAV-based sensor, which is incapable of penetrating the gaps between leaves to record the woody parts hidden behind the foliage, the feasibility of reconstructing trees using QSM is doubtful.

According to the study of Miller et al. (2015), there are also some external factors that cause ambiguous 3D information extracted by UAV images: poor camera resolution or the images being captured too far away from the tree, which will provide an insufficient amount of pixels in the imagery to create recognizable features; direct sunlight might lead to over-exposed images and shadows; the change in the sun's azimuth, as well as surface albedo, could also affect the model quality if the image acquisition period is too long; and windy conditions will cause too much movement in the leaves and small branches. The internal attributes such as the complexity of tree structure will cause the shadow and occlusion problem in UAV images as well (Shahbazi, Sohn, Théau, & Menard, 2015). As a result, the oblique image which is capable of viewing objects from different perspectives can be used to expose the blind spots to some extent in the study of the windbreak (Lin et al., 2015).

This research aims to investigate the feasibility of reconstructing the QSM of windbreaks as well as single trees by using a UAV-derived point cloud during the leaf-on season and leaf-off season. It also studies the influences of oblique camera angles for point cloud generation. QSM is expected to be successfully reconstructed based on the point cloud with the best quality.

The conceptual diagram is shown in Figure 8, which shows the key elements and operations involved in this study.

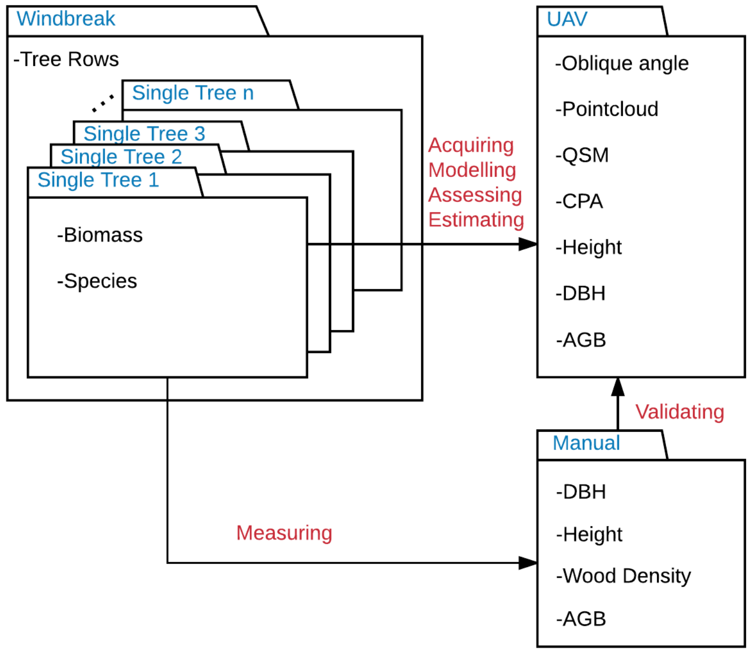

Figure 8. Conceptual diagram

1.3. Research objectives

The overall objective of this research is to assess the potential of the UAV point cloud as input in QSM for AGB estimation of windbreaks and single trees.

Specific objectives:

1. To identify the optimal oblique camera angle of UAV flights for point cloud generation as input in QSM.
2. To estimate DBH through QSM, UAV point cloud and CPA regression model, compare their accuracy to field measured DBH during the leaf-on season and leaf-off season, respectively.
3. To estimate tree height through QSM and UAV point cloud, compare their accuracy to reference height extracted from Aerial Laser Scanning (ALS) data during the leaf-on season and leaf-off season, respectively.
4. To estimate AGB using QSM volume and compare its accuracy with AGB calculated through tree allometry during the leaf-on season and leaf-off season, respectively.
5. To compare the different approaches.

1.4. Research question and hypothesis

The research questions and hypothesis are shown in Table 1. Figure 9 is the dendrogram of research questions for better understanding.

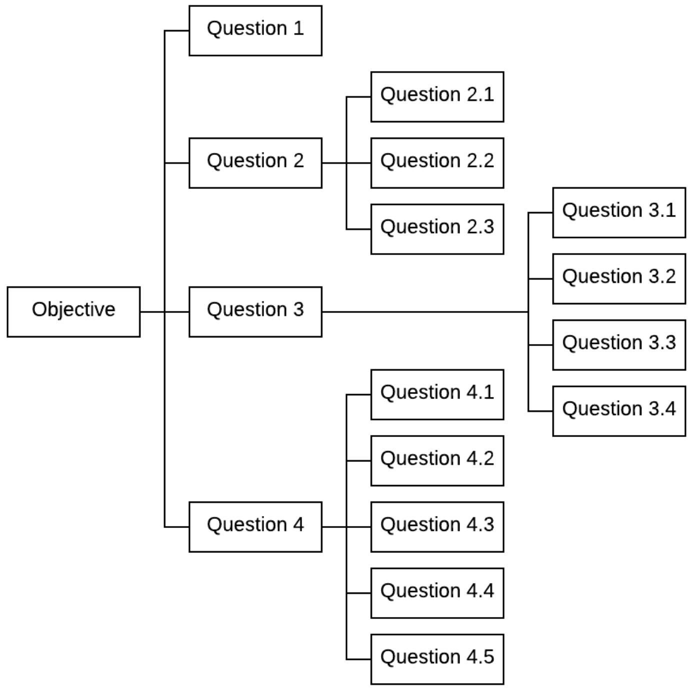

Figure 9. Dendrogram diagram of research questions.

Table 1. Research question and hypothesis

Research question		Hypothesis
1. Do oblique camera angles of UAV flights influence the point cloud density and completeness of individual tree?		• H_0: Different oblique camera angles of UAV images do not influence the point cloud density and completeness of individual trees. • H_a: Different oblique camera angles of UAV images influence the point cloud density and completeness of individual trees.
2. Is there a significant difference between the UAV point cloud-derived DBH, QSM-derived DBH, CPA-estimated DBH and the reference DBH?	2.1. Is there a significant difference between DBH derived from the UAV point cloud and DBH from field measurements?	• H_0: There is no statistically significant difference between DBH derived from the UAV point cloud and DBH derived from the field. • H_a: There is a statistically significant difference between DBH derived from the UAV point cloud and DBH derived from the field.
	2.2. Is there a significant difference between DBH derived from the QSM and DBH from the field measurements?	• H_0: There is no statistically significant difference between the DBH derived from QSM and DBH derived from the field. • H_a: There is a statistically significant difference between DBH derived from the QSM and DBH derived from the field.

Research question		Hypothesis
	2.3. Is there a significant difference between DBH estimated by CPA and DBH from the field measurements?	• H_0: There is no statistically significant difference between DBH estimated by CPA and DBH derived from the field. • H_a: There is a statistically significant difference between DBH estimated by CPA and DBH derived from the field.
3. Is there a significant difference between the UAV point cloud-derived height, QSM-derived heights, and the reference heights?	3.1. Is there a significant difference between height derived from the UAV point cloud and height from the ALS?	• H_0: There is no statistically significant difference between tree height derived from the UAV point cloud and ALS height. • H_a: There is a statistically significant difference between tree height derived from the UAV point cloud and ALS height.
	3.2. Is there a significant difference between height derived from QSM and height from ALS?	• H_0: There is no statistically significant difference between tree height derived from QSM and ALS height. • H_a: There is a statistically significant difference between tree height derived from QSM and ALS height.
	3.3. Is there a significant difference between height derived from the UAV point cloud and height from the Laser Distance Measurer in the field?	• H_0: There is no statistically significant difference between tree height derived from the UAV point cloud and tree height obtained by Laser Distance Measurer. • H_a: There is a statistically significant difference between tree height derived from the UAV point cloud and tree height obtained by Laser Distance Measurer.
	3.4. Is there a significant difference between height derived from QSM and height from Laser Distance Measurer in the field?	• H_0: There is no statistically significant difference between tree height derived from QSM and tree height derived by the Laser Distance Measurer. • H_a: There is a statistically significant difference between tree height derived from QSM and tree height derived by the Laser Distance Measurer.
4. Is there a significant difference between the AGB calculated by the QSM volume, the AGB calculated by allometry using DBH (estimated by	4.1. Is there a significant difference between AGB calculated by QSM volume and AGB calculated by allometry using DBH (estimated by CPA) and UAV-point cloud height as input?	• H_0: There is no significant difference between AGB calculated by QSM volume and AGB calculated by allometry using DBH (estimated by CPA) and UAV-point cloud height. • H_a: There is a significant difference between AGB calculated by QSM volume and AGB calculated by allometry using DBH (estimated by CPA) and UAV-point cloud height

Research question		Hypothesis
CPA) and UAV-point cloud height as input, the AGB calculated by point cloud-derived DBH and height, the AGB derived from allometry that uses QSM-derived DBH and height, and the AGBs calculated by allometry that use reference DBH and height as input?	4.2. Is there a significant difference between AGB calculated by QSM volume and AGB derived from allometry that uses UAV-derived DBH and height as input?	• H_0: There is no significant difference between AGB estimates calculated by QSM volume and AGB estimates derived from allometry that uses UAV-derived DBH and tree height. • H_a: There is a significant difference between AGB estimates calculated by QSM volume and AGB estimates derived from allometry that uses UAV-derived DBH and tree height.
	4.3. Is there a significant difference between AGB calculated by QSM volume and AGB derived from allometry that uses QSM-derived DBH and height as input?	• H_0: There is no significant difference between AGB estimates calculated by QSM volume and AGB estimates derived from allometry that uses QSM-derived DBH and tree height. • H_a: There is a significant difference between AGB estimates calculated by QSM volume and AGB estimates derived from allometry that uses QSM-derived DBH and tree height.
	4.4. Is there a significant difference between AGB calculated by QSM volume and AGB derived from allometry that uses field derived DBH and ALS height as input?	• H_0: There is no significant difference between AGB estimates calculated by QSM volume and AGB estimates derived from allometry that uses field-derived DBH and ALS tree height. • H_a: There is a significant difference between AGB estimates calculated by QSM volume and AGB estimates derived from allometry that uses field derived-DBH and ALS tree height.
	4.5. Is there a significant difference between AGB calculated by QSM volume and AGB derived from allometry that uses field-derived DBH and height obtained by Laser Distance Measurer as input?	• H_0: There is no significant difference between AGB calculated by QSM volume and AGB derived from allometry that uses field-derived DBH and height obtained by Laser Distance Measurer. • H_1: There is a significant difference between AGB calculated by QSM volume and AGB derived from allometry that uses field-derived DBH and height obtained by Laser Distance Measurer.

2. METHODOLOGY

2.1. Study area

The study area is selected based on the airspace restrictions and the spatial appearance of trees. Areas that have trees planted in a linear shape with flight clearance are preferred.

In the study area, which is shown in Figure 10, trees are planted along the road inside a park in Gronau- the town belongs to the German province of North Rhein-Westfalen. In addition, the studied tree species is American sweetgum (*Liquidambar styraciflua*).

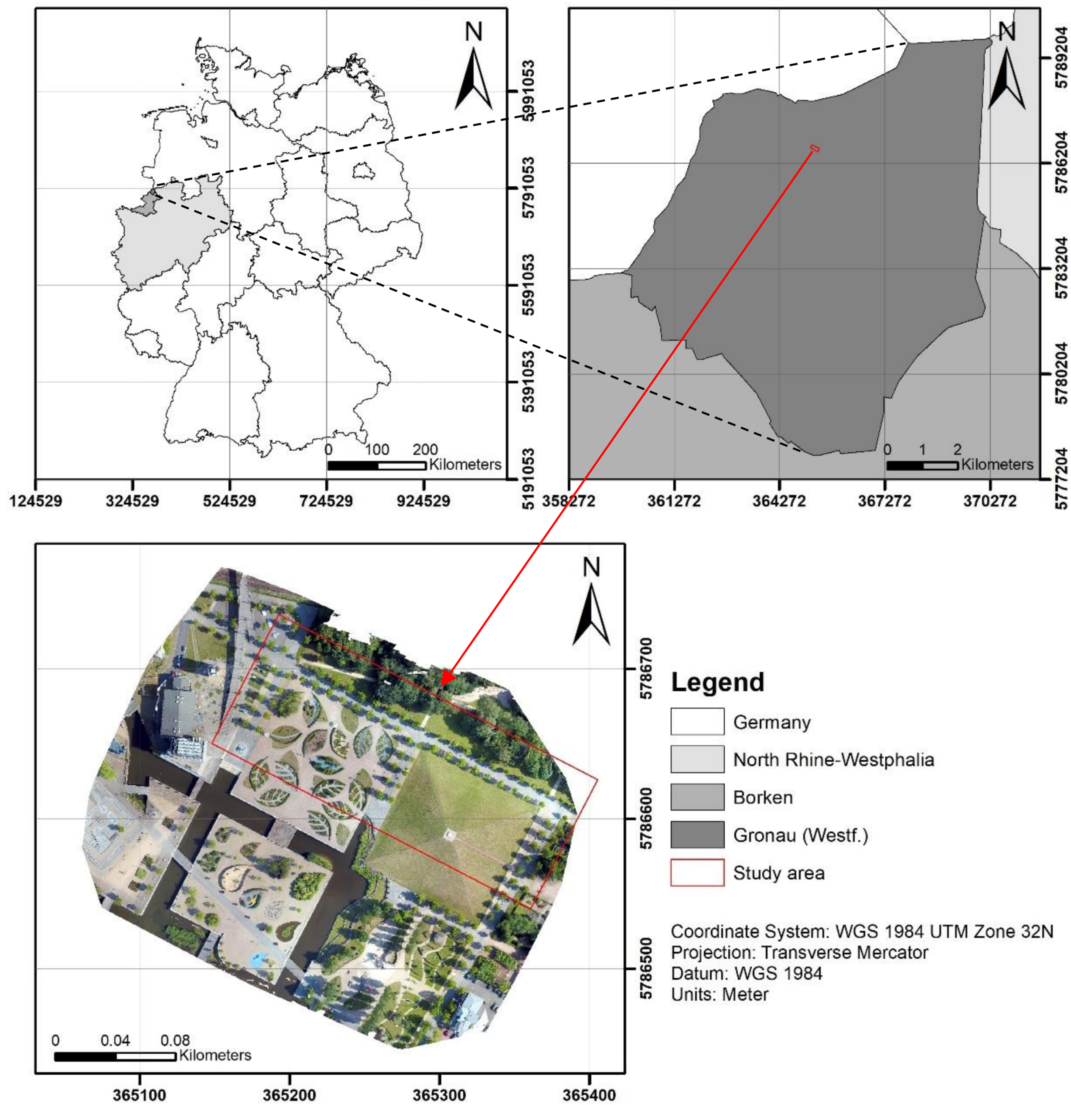

Figure 10. The study area in Germany. The background orthophoto was acquired in July 2017 and provided by the University of Twente. The orthophoto was generated using nadir images obtained by DJI Phantom 4, with a 50m flight height, 80% forward overlap and 70% side overlap.

2.2. Workflow

The workflow of this research is demonstrated in Figure 11. The main steps consist of data collection and pre-processing, data processing, data analysis.

Two datasets were collected during the data collection phase: reference data and UAV point cloud data. During the manual data acquisition, DBH and the height of each tree in the study area were measured using different tools, while the Aerial Laser Scanning (ALS) heights of each tree were extracted from the Canopy Height Model (CHM). For UAV data acquisition, Question 1 was answered by testing oblique flight angles. Structure from Motion technique was used for generating the dense point cloud from the images. Then, the sampled trees and their property values, for instance, DBH, height, and CPA, were extracted from the dense point cloud during the pre-processing sub phase.

For the processing procedure, the extracted point clouds of individual trees were used for the 3D QSM. In addition, the vegetation parameters of individual trees obtained after the tree model reconstruction were used for the biomass calculation and further accuracy assessment in the analysis phase to answer Questions 2, 3 and 4.

The detailed flow of this study will be described in sections 2.3, 2.4, 2.5, 2.6 and 2.7.

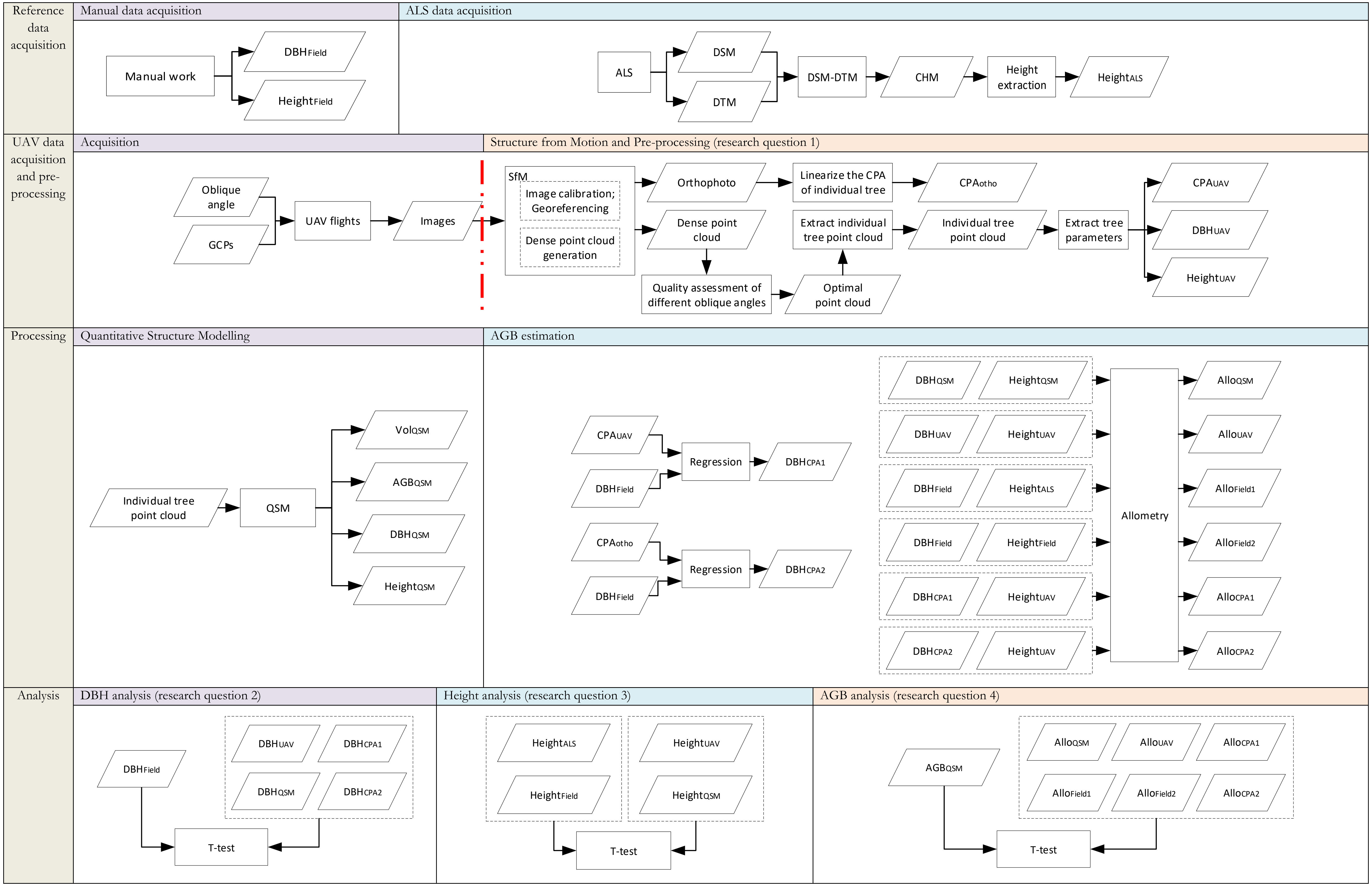

Figure 11. Research workflow.

2.3. Data collection and pre-processing

The data collection procedure comprises 2 main parts: reference data acquisition, and UAV data acquisition and pre-processing.

2.3.1. Reference data acquisition

The sampling strategy of this study was to collect field data from all trees within the study area since the study object was individual trees. DBH (1.30 m from the base of the tree trunk) and tree height ($Height_{Field}$) were manually measured with specific instruments and used for result validation during the analysis procedure.
The instruments for manual data acquisition and their usages are shown in Table 2.

Table 2. Instruments and usage

Instruments	Usage
Map of study area	Orientation
Diameter tape	Measure DBH of individual trees
Leica Disto™ D510	Measure tree height

The diameter of 10 cm was determined as the threshold value for the measurement, only trees with a diameter equal to or above 10 cm were recorded, since the biomass contribution of trees with a diameter under 10 cm is negligible (Brown, 2002).
In addition, reference height ($Height_{ALS}$) was extracted from the ALS data because of the uncertainty of manual height measurements due to occlusion caused by nearby trees, which made it difficult to determine the top and the bottom of the tree in one measurement. CHM was generated from the ALS data by subtracting the Digital Terrain Model (DTM) from Digital Surface Model (DSM). Although the ALS showed an underestimation approximately 7-8% based on the work of Suárez et al. (2005), the accuracy was still good enough to evaluate the estimated value. The DSM and DTM were provided by Geobasisdaten der Kommunen und des Landes Nordrhein-Westfalen (NRW), and the detailed information is shown in Table 3.

Table 3. Description of the ALS data

Data	Point density	Accuracy of elevation	Source
DTM	1-4 points/m²	+/- 20 cm	Bezirksregierung Köln (2016a)
DSM	1-4 points/m²	+/- 20 cm	Bezirksregierung Köln (2016b)

2.3.2. UAV data acquisition

The UAV based images were acquired using the DJI Phantom 4 on 4 October 2017 (leaf-on season) and the DJI Phantom 4 Pro on 1 December 2017 (leaf-off season), both with an RGB camera onboard. The specifications of the camera are shown in Table 4 and Table 5.

Table 4. DJI Phantom 4 camera and image parameters

Camera model	FC330_3.6_4000x3000 (RGB)	
Image coordinate system	Datum	World Geodetic System 1984
	Coordinate System	WGS 84 (egm96)
Horizontal image accuracy [m]	5.000	
Vertical image accuracy [m]	10.000	
Pixel size [μm]	1.57937	

Table 5. DJI Phantom 4 Pro camera and image parameters

Camera model	FC6310_8.8_4864x3648 (RGB)	
Image coordinate system	Datum	World Geodetic System 1984
	Coordinate System	WGS 84 (egm96)
Horizontal image accuracy [m]	5.000	
Vertical image accuracy [m]	10.000	
Pixel size [μm]	2.34527	

Before the UAV flight, Ground Control Points (GCPs), which could be clearly viewed during the flight, were selected and marked. The accurate locations of GCPs were recorded with the help of differential GNSS (Leica CS15).

During the UAV data acquisition procedure, images with different oblique camera angles were collected to determine the optimal angle for point cloud generation. However, the crown size and the oblique camera angle can cause an occlusion problem in the acquired UAV images, which can be seen in Figure 12. As a result, there is no point generated in certain parts of the tree which hide behind the tree crown in the UAV images. In addition, SfM uses corresponding points appeared in separate images to recover its spatial information, the quality of the final products might be reduced if the easily identified features are occluded by foliage, which is difficult to differentiate.

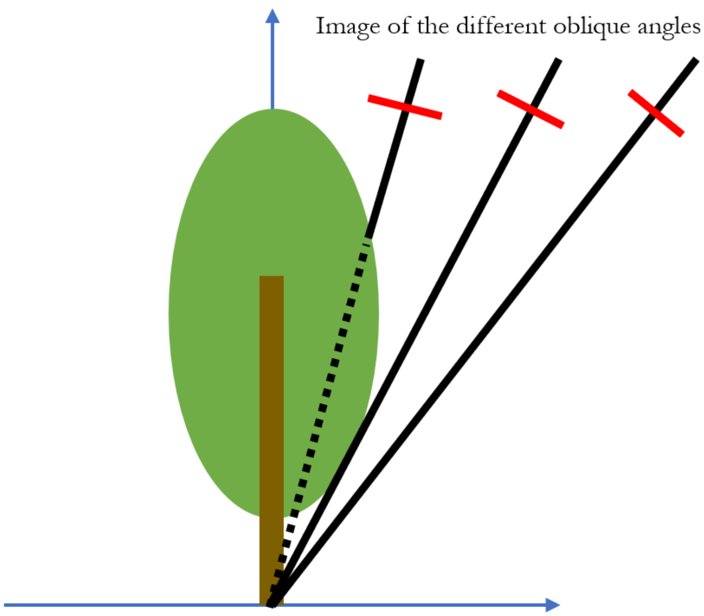

Figure 12. Occlusion problem caused by different oblique camera angles. Image A shows the occlusion problem caused by the canopy, while image B and C capture the woody parts of the tree at the image centre.

The occlusion leads to the unsuccessful reconstruction of QSM. Thus, the threshold for the oblique camera angle was calculated before the UAV flight to avoid the useless data. The profiles of the crowns are assumed to have two shapes, as demonstrated in Figure 13; one shape is an ellipse, and the other is a semi-ellipse. Consequently, the minimum oblique angle is determined when the line, which connects the camera with the tree base area, touches the crown ellipse or semi-ellipse. The calculation of the minimum oblique angle is shown in Figure 13. The camera oblique angle of the elliptical crown is calculated based on the equation of an ellipse:

$$\frac{x^2}{b^2} + \frac{(y-a-c)^2}{a^2} = 1$$

Although the camera with an oblique angle that exceeds the threshold might also record the trunk information near the base area, the distortion could be so large that it influences the image matching in SfM (Liu, Guo, Jiang, Gong, & Xiao, 2016).

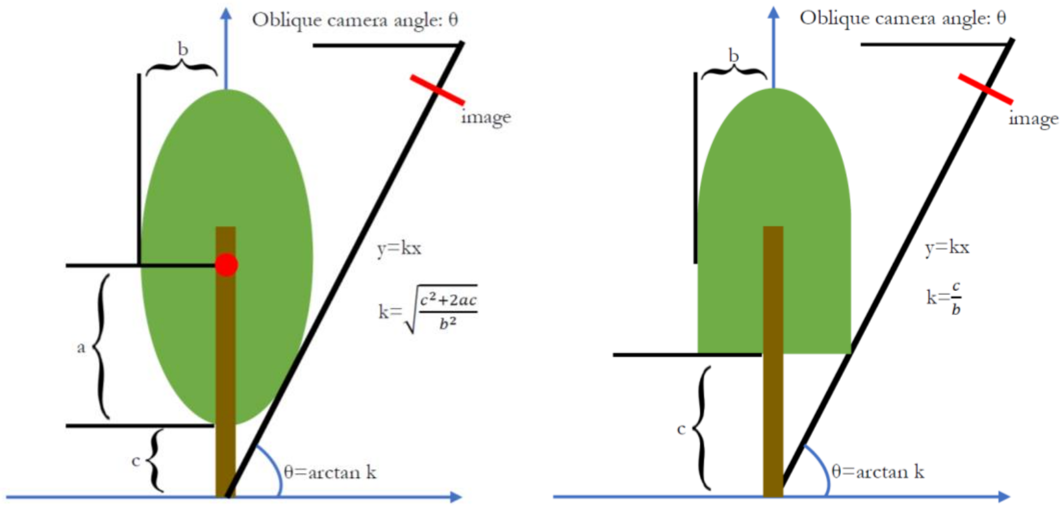

Figure 13. The crown profile and minimum oblique angle of the UAV image.

After the preliminary field visits and calculation, the oblique angles were set at 35°, 40°, 45°, and 50°. During the leaf-on season, for each oblique angle, two inverse double-grid pattern flights were carried out to make sure the tree structure could be recorded at as many perspectives as possible (Fritz et al., 2013). For a clearer understanding, two inverse one-grid pattern flights are shown in Figure 14 A.

A:

B:

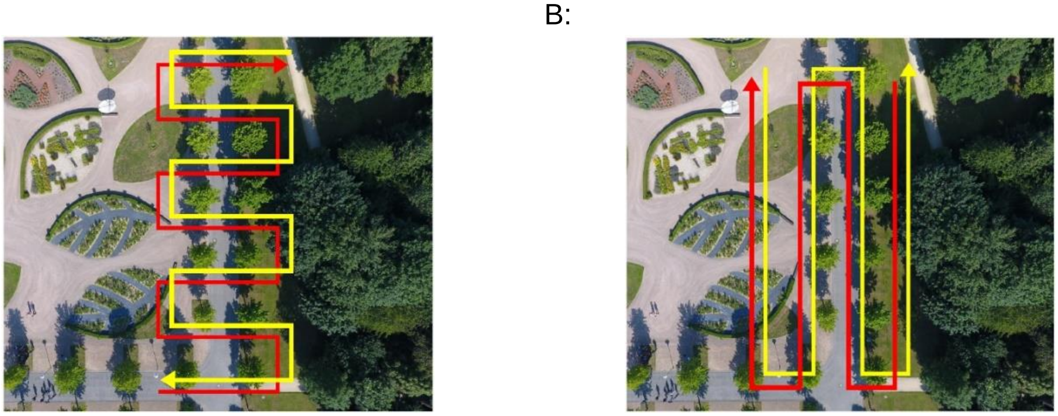

Figure 14. Two inverse one-grid flights. Background image source: University of Twente.

Processing the images acquired during leaf-on season showed a negative result caused by high wind speed and moving leaves. The quality of the point cloud of the four oblique angles was too poor to reconstruct an accurate model. Thus, two paired flights were carried out during leaf-off season at oblique camera angle of 35°, 40°, 45°, and 50°; the two paired flights were perpendicular to each other and were the combination of Figure 14 A and Figure 14 B. However, except for the from 50° oblique camera angle of one paired flight (Figure 14 A), all the other datasets were not available because of an unreliable SD card and the poor flight conditions, such as the high wind speed and the cloudy weather. No extra flight could be carried out to compensate for the unsaved missions due to the time limitation and weather.

The flight height was approximately 20 metres above the crown for each sample to guarantee the flight safety and the high quality of the images. During the flight missions, the overlap parameter was set to 75% for the side and 90% for the forward during the leaf-on season; and 70% for the side and 90% for the forward during the leaf-off season. The overlap parameter setting was limited by the duration of the UAV battery; the overlap rates were the maximum values within 15 minutes of the battery duration to ensure the safety of the drone.

2.3.3. Structure from Motion and pre-processing of the UAV point cloud

Structure from Motion (SfM)

After the UAV image acquisition, the Structure from Motion (SfM) method was used to construct a dense point cloud as well as an ortho-mosaic. The process of SfM was implemented automatically using Pix4D software with some possibly necessary manual edits/corrections, such as importing the GCPs and manually marking the GCPs in multiple images. The marked GCPs were used as additional tie-points (matching feature points) for improving image calibration. GCPs with georeferences were utilised for refining the geo-referencing of the 3D point cloud.

One thing should be noted is that the resolution of oblique image is not uniform. Lingua, Noardo, Spanò, Sanna, & Matrone (2017) use the following relations (1), (2), (3) and (4) to compute the resolution of the image at the minimum distance (d_A) and maximum distance (d_B) of the camera to the object (Figure 15):

$$d_M = \frac{h}{\cos\alpha} \quad (1)$$

$$d_A = \frac{h}{\cos(\alpha - \beta_y)} \quad (2)$$

$$d_B = \frac{h}{\cos(\alpha + \beta_y)} \quad (3)$$

$$\text{Resolution} = \frac{d * S_{pix}}{c} \quad (4)$$

where:

h = flight height
α = 90° - oblique camera angle
c = focal length,
d = considered distance
S_{pix} =the pixel size

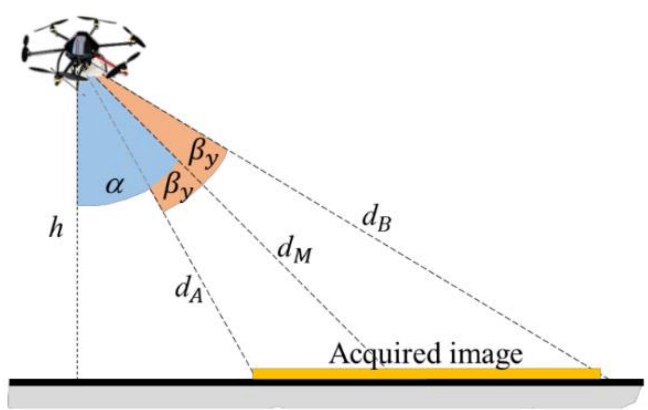

Figure 15. Geometry of an oblique image acquired from a UAV (Lingua et al., 2017)

Thus, for the part that is closer to the camera, the resolution is higher, and more feature points are detected and matched. For the part that is farther from the camera, the conditions are reversed.

Quality assessment of different oblique angles

The point density was checked based on the quality reports which were generated automatically by the Pix4D software.

Pre-processing of the UAV orthophoto and point cloud

The orthophoto was one of the products from the Structure from Motion process. In this study, two CPA datasets were collected; the dataset CPA_{UAV} dataset was manually delineated based on the nadir image generated orthophoto (Figure 16 B) since the orthophoto was a geometrically corrected image with a uniform scale. The CPA_{otho} dataset was generated by converting the individual tree point cloud (Figure 16 A1) from the leaf-on season into a raster (Figure 16 A2) from the top-down view.

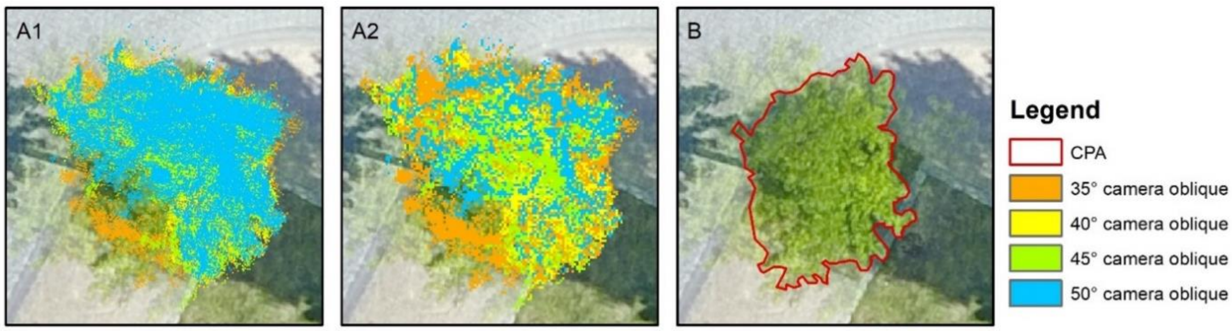

Figure 16. Two types of CPA datasets. Image A1 is the individual tree point cloud, A2 is the rasterization of the individual tree point cloud, and B is the CPA digitalisation based on the orthophoto. The background orthophoto was acquired in July 2017 and provided by the University of Twente.

Although the leaf size of the Sweetgum was approximately 10 cm to 15 cm by visual inspection in the field, the cell size of the rasterization was set to 5 cm*5 cm. As shown in Figure 17, the star-shaped leaf is divided by a 10*10 fishnet, but the leaf only covers 25 cells— 1/4 of the 10*10 fishnet. Thus, 5 cm *5 cm was the leaf size approximation of the studied species.

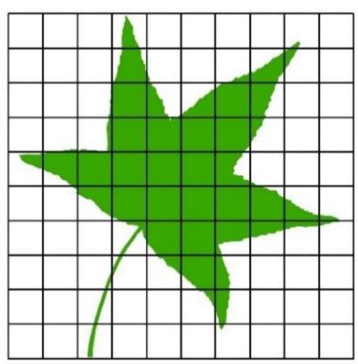

Figure 17. The Sweetgum leaf.

The cell number of the tree crown (N) was counted and used for individual tree CPA calculations with the equation:

$$CPA(m^2) = N*0.05*0.05$$

The individual tree was manually extracted in the CloudCompare software after generation of the dense point cloud. To extract the DBH from the UAV point cloud, a circle was fitted to the point cloud at 1.3 m above the base of the tree. Each cluster of 10 cm thickness from 1.25 m to 1.35 m of the individual tree was used as the input for circle fitting to ensure the sufficiency of points (Tansey, Selmes, Anstee, Tate, & Denniss, 2009).

The approach for DBH circle fitting was the principle of least square adjustment. The best-fitted circle of DBH was estimated by minimising the distance from the circle to the points of the point cloud with the iterative operation (Richard Brown, 2007).
The tree height was determined by measuring the vertical distance between the lowest point and the highest point of the individual tree point cloud in the software CloudCompare software.

2.4. QSM

The QSM reconstruction by using the UAV point cloud consists of the following three steps: noise filtering, topological reconstruction of the branching structure and geometrical reconstruction of the branch surfaces.

2.4.1. Noise filtering

Noise filtering must be performed before the reconstruction of the tree model when the input data are UAV point clouds. The noise caused by certain problems, such as swinging of branches, blurred images, and inaccurate image calibration, will not be used for the reconstruction of the real surface of the tree model. During the leaf-on season, leaves are a large part of the individual tree point cloud, while one of the main assumptions of QSM is " the whole tree is wood" (Raumonen, 2017). Hence, the filtering process can have a significant influence on the model reconstruction by separating leaves and wood. Although the noise problem caused by leaves is eliminated during the leaf-off season, the unstable image acquisition of UAV due to wind may increase the number of noise points as well. As a result, the noise filtering process was carried out for the leaf-on season dataset and leaf-off season dataset.
There are two filtering schemes in this procedure. One is used to remove the noise or isolated points by defining a small ball for each point and rejecting the ball that contains too few points. The other is used to delete small separate parts of the point cloud. A larger ball is used to determine the component connectivity of the point cloud; after that, the disconnected components will be removed. In Figure 18, the point p and q are defined as connected because of the existence of overlapping balls, while point v and w are unconnected without the overlapping balls.

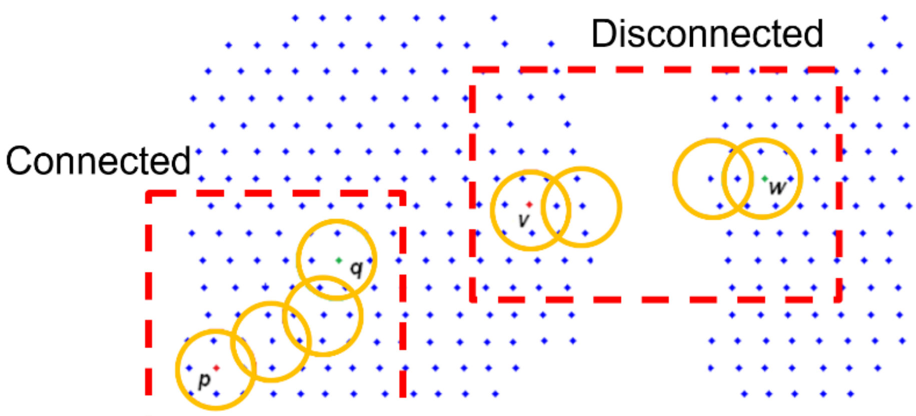

Figure 18. The definition of connected components (Raumonen, Kaasalainen, Kaasalainen, & Kaartinen, 2011). Point p and q are connected, v and w are disconnected.

The filtering-parameter setting and the quality of the filtered point cloud rely on the noise level and its distribution in the dataset; therefore, no rule exists for the parameters setting (Raumonen et al., 2013). In this research, parameters were tested with a trail tree to obtain appropriate filtering result. The radius of the balls for noise removal used in the filtering process was gradually increased from 0.01 m, and the filtering results were evaluated by visually inspecting the structure of the filtered point cloud. It was found that 0.07 m was the optimal value for the leaf-on season and 0.03 m was optimal for the leaf-off season since the noise point was almost eliminated, and the tree structure was correct.

2.4.2. Topological reconstruction of the branching structure

The step aims to segment the point cloud into stems and individual branches. There are several steps in the method for the segmentation of the point cloud as follows: cover set generation, tree set generation, and segmentation and segmentation correction.

2.4.2.1. Cover sets

Cover sets are small subsets of the individual tree point clouds. This is the basis of segmentation and is observed as small patches of the tree surface. The cover sets are the smallest "unit" for segmenting the point cloud into branches and a trunk (Figure 19). In addition, the parameters *PathcDiam*, *BallRad*, and *nmin* are used to generate the random sets where:
PathcDiam: patch size of the uniform-size cover set;
BallRad: ball size used for cover set generation; and
nmin: minimum number of points inside the ball.
A trail tree was used to find the optimal parameters by visual inspection. Two different covers are introduced in this method. The first cover is used to remove the points that do not belong to the tree and obtain the primary segments for the generation of the second cover set. The second cover uses the priori information provided by the first cover to determine the size and the neighbour-relation with adjacent covers.
The cover set should be not only small enough for recording the local details such as the tip and base of the individual branches but also be large enough for efficient and correct segmentation.

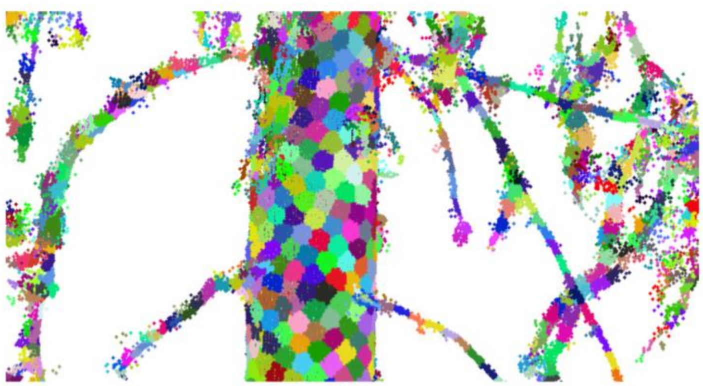

Figure 19. A cover is a partition (Raumonen et al., 2013). Different colours indicate different cover sets. And the size of the cover set is uniform.

2.4.2.2. Tree sets

After the generation of the first cover, there are several things to do before the following segmentation that aims to separate branches and stems. First, eliminate the non-tree points, for example, the ground point and understory point. Second, determine the starting point of segmentation—the base of the stem. Finally, connect the cover sets to form the whole tree structure considering the neighbour-relation. However, there are often many gaps among the cover sets caused by occlusion; thus, a "bridge over" operation should be carried out by modifying the neighbour-relation to ensure the connectivity of the tree structure. Therefore, for the second cover set, the non-tree points must already be removed, and the neighbour-relation of the new cover sets should be used to obtain the whole tree, which is a single connected whole (Raumonen, 2017).

2.4.2.3. Segmentation and correction

The branches and stem can be separated by segmentation. This process is used to obtain segments without bifurcation by assessing the local connectivity. The starting point is the base of the trunk, and the whole point cloud of the individual tree will be segmented in a step-by-step process along the stem and then along the branches. The possible bifurcations are determined first, and its base will be saved as a new basis for later segmentation. After that, the same process will repeat at the first bifurcation found from its base to the tip.

However, the segmentation process may end abruptly because it incorrectly determines the bifurcation point. Thus, a correction should be conducted to ensure that the segmentation reflects the real world as much as possible. This step is known as segmentation correction, and the theory is "The tip of the branch is the tip among all the tips of the child segments that is the furthest away from the base of the branch" (Raumonen, 2017).

2.4.3. Geometrical reconstruction of the branch surfaces

The final step of QSM fits locally approximated cylinders around the segments to reconstruct the tree model concerning the topological relation. Least squares fitting is used in this procedure. However, some modifications, such as eliminating the extreme value of the branch radii and filling the gaps between the child and parent segments, should be performed to avoid the wrong reconstruction. To eliminate extreme values of the branch radii, the following optional controls can be implemented: define the outliers of the least squares fit, and removed points that are much farther from the axis than the estimated radius to ensure the fitted cylinders are not too large. There are also constraints used to avoid the unnatural varying radii of the branch-the child branch should be thinner than the parent branch, and the radii of the branch gradually decrease towards the tip (Raumonen, 2017). Then, the cylinder fit for the branch data was computed, including the length, volume, and angle of each branch, in the function branches. Consequently, tree measurements such as DBH, height, and volume can be easily derived from the model.

2.4.4. Implementation

The QSM was run five times with the same input parameters for each tree. The reason for this was to avoid the influence of randomness—the cover set was generated randomly in each run (Raumonen et al., 2013). The average value of the results of the five runs, such as DBH, height, and volume, was calculated for future analysis.

2.5. Regression analysis and validation of CPA and DBH

The regression analysis describes how dependent variable changes with explanatory variable. The purpose of the regression analysis is to predict the dependent variable, given the relationship between dependent variable and explanatory variable. In this study, DBH was the dependent variable and CPA was the independent variable, DBH was estimated by using the regression relationship between DBH and CPA.

A simple linear regression (y= a+b*x) was used in this study to determine the regression coefficient that indicates the strength and the sign of the relationship between CPA and DBH. Shah et al. (2011) found there was a linear relationship between CPA and DBH.

The dataset was randomly divided into two parts: 60% for model calibration and 40% for validation (Gill, Biging, & Murphy, 2000). Root mean square error (RMSE) was used for assessing the predictive accuracy of the model, the calculation was shown in Table 6 below (Shah et al., 2011):

Table 6. Statistics used to assess the regression

Statistics	Formula	Remarks
RMSE	$\sqrt{\frac{\sum_{i=1}^{n}(Y_i - \hat{Y}_i)^2}{n}}$	Y_i is measured value, $\hat{Y}_i$ is the predicted value
RMSE in %	$\frac{RMSE}{\bar{Y}} \times 100\%$	$\bar{Y}$ is the mean of validation dataset

2.6. Allometry and wood density

To estimate the biomass, the tree volume and biomass were calculated with the allometric equation created by Williams & Gresham (2006). The sampled American sweetgums (*Liquidambar styraciflua*) for developing these allometric equations were planted in rows on marginal agricultural land near Bainbridge, GA in the USA and were managed to eliminate all limitations of tree growth except light, temperature and intra-specific competition (Williams & Gresham, 2006). The equation and specific parameters for volume and biomass calculation are shown in Table 7:

Table 7. Allometric equations for biomass estimation (Williams & Gresham, 2006)

Data	R^2
Trunk volume = $0.0000339d^2h+0.00263$	0.958
Total biomass = $0.0305\ d^2h+3.788$	0.958

The abbreviations are as follows: $d^2h=DBH^2\times height$. The unit of diameter is cm; height, m; and volumes, m^3. The trunk volume, in this case, was calculated to a 5-cm top, and the 5-cm top was somewhere within the uppermost metre (Williams & Gresham, 2006). Figure 20 explains the 5-cm top. The total biomass refers to the AGB since the trees were cut at ground line, and only the above ground part was used to develop the allometric equation.

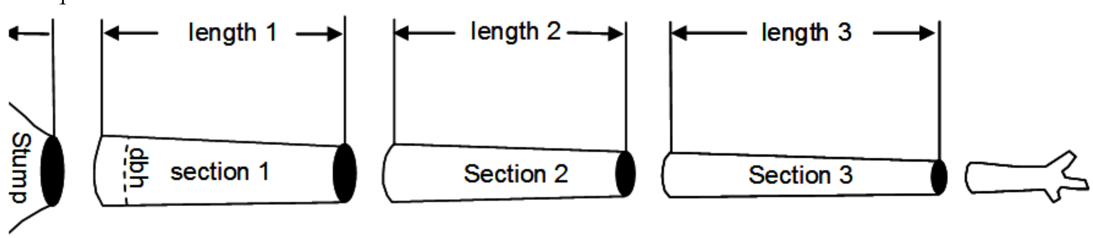

Figure 20. Subdivision of a trunk into sections ("Stem volume," 2013). Sections 1, 2 and 3 will be used for volume calculation. For the remaining parts, the stump is not included in the trunk volume; the top section, with a length of less than 5 cm, is excluded as well (Williams & Gresham, 2006).

The density of oven dry biomass per fresh volume is extracted from the database of global wood density; the density of Sweetgum (*Liquidambar styraciflua*) is 460 kg/m3 (Chave et al., 2005; Zanne et al., 2009).

2.7. Analysis

Figure 21 illustrates the general steps for the analysis of the research questions 1 – 4. The confidence level of 95 % (α = 0.05) will be used in all analysis steps.

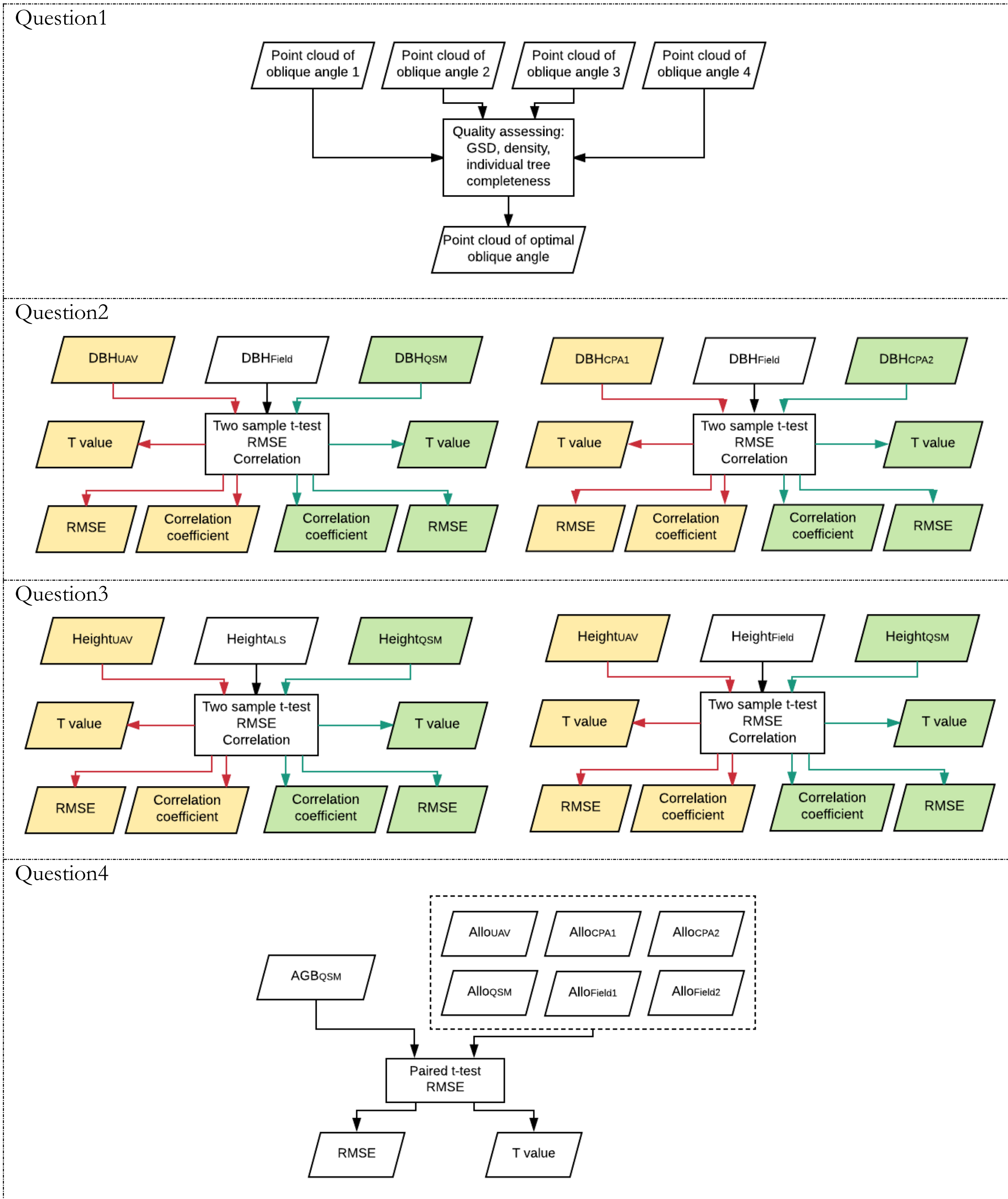

Figure 21. Data analysis steps for research questions 1- 4. The same colour indicates the corresponding input and output.

Question 1: Do oblique camera angles of UAV flights influence the point cloud density and completeness of individual trees?

The point density is calculated and recorded automatically during the Structure from Motion process. The value of the parameter was compared after the process by looking through the quality report. However, the points are not uniformly distributed in the UAV point cloud because the points are densified based on the irregularly distributed tie points, and the feature point is detected based on the texture. Rosnell & Honkavaara (2012) evaluated the point densities of the following five different surface types: field, forest, grass, asphalt road and gravel road windows. Also, the result showed that the density of homogeneous objects (e.g., asphalt surfaces) was lower than that of the heterogeneous objects because it's difficult to extract and match feature points on the smooth/homogeneous surface (Mancini et al., 2013). As a result, the point density cannot be directly used to indicate the completeness of individual trees. Thus, ten trees for each oblique angle were extracted, the number of the individual tree points in the cloud was counted, and a QSM was reconstructed to make the comparison.

Question 2: Is there a significant difference between the UAV point cloud-derived DBH values, QSM-derived DBHs, CPA-estimated DBH, and the reference DBH?

Question 3: Is there a significant difference between the UAV point cloud-derived height values, QSM-derived heights, and the reference heights?

Question 2 and Question 3 are put forward to determine the relationship between two kinds of independent samples: the estimated value obtained from different methods and the ground truth value measured by reliable instruments. Therefore, a two-sample t-test was used in this case to answer the questions.

The hypothesis for the independent t-test is:

$$H_0: \bar{x}_{reference} = \bar{x}_{estimated}$$

$$H_a: \bar{x}_{reference} \neq \bar{x}_{estimated}$$

The equation for the independent t-test is:

$$\text{t-statistic} = \frac{\bar{x}reference - \bar{x}estimated}{\sqrt{\frac{s^2_{reference}}{n_{referenc}} + \frac{s^2_{estimated}}{n_{estimated}}}}$$

The abbreviations are as follows: $\bar{x}$ is the mean of the samples, s^2 is the variance and n is the number of samples (Philip Rowe, 2007).

Question 4: Is there a significant difference between the AGB calculated by a) the QSM volume, b) the AGB calculated by allometry using DBH (estimated by CPA) and UAV-point cloud height as input, c) the AGB calculated by point cloud-derived DBH and height, d) the AGB derived from allometry that uses QSM-derived DBH and height, and e) the AGBs calculated by allometry that use reference DBH and height as input?

Question 4 is answered by using a paired t-test to compare the biomass estimates of the same individual tree. The purpose of the paired t-test is to determine whether the mean difference between paired values is significantly different from 0.

The hypothesis for the paired t-test is:

$$H_0: \bar{x}(reference\text{-}estimated) = 0$$

$$H_a: \bar{x}(reference\text{-}estimated) \neq 0$$

The equation for the independent t-test is:

$$\text{t-statistic} = \frac{\bar{x}(reference - estimated) - \mu_0}{\frac{S}{\sqrt{n}}}$$

The abbreviations are as follows: $\bar{x}$ is the mean of the samples, μ_0 is the hypothesis mean (0), S is the standard deviation of the samples and n is the number of samples (Philip Rowe, 2007).

Equations (1), (2), and (3) are used to calculate the model bias (in %) for assessing the accuracy of different biomass estimation methods (Gonzalez de Tanago Menaca et al., 2017). Here, AGB calculated by allometry that uses the field-measured DBH and height ($\mathrm{Allo}_{\mathrm{Field2}}$) is used as a reference.

$$\mathrm{AGB}_{\mathrm{estimation\ errors}} = \mathrm{AGB}_{\mathrm{model}} - \mathrm{AGB}_{\mathrm{Reference}} \quad (1)$$

$$\text{Relative error (\%)} = \left(\frac{\mathrm{AGB}_{\mathrm{model}} - \mathrm{AGB}_{\mathrm{Reference}}}{\mathrm{AGB}_{\mathrm{Reference}}}\right) \times 100 \quad (2)$$

$$\text{Model bias (\%)} = \left(\frac{\sum_1^n \mathrm{AGB}_{\mathrm{estimation\ errors}} \div n}{\text{Mean }\mathrm{AGB}_{\mathrm{Reference}}}\right) \times 100 \quad (3)$$

3. RESULTS

3.1. Reference data acquisition

During the reference data acquisition procedure, a total number of 76 trees were sampled in the field. The species of the sampled trees is American Sweetgum (*Liquidambar styraciflua*). Table 8 shows the summary statistics for the reference data.

Table 8. Statistical information of the reference data

	Field-measured DBH(m)	ALS height(m)	Laser scanner measured height(m)
Maximum	0.301	9.54	12.5
Minimum	0.115	4.69	6.91
Mean	0.197	7.19	9.68
Median	0.195	7.20	9.68
Standard deviation	0.031	0.95	1.20

ALS tree height was extracted from the Canopy Height Model. The new generated Canopy Height Model is shown in Figure 22.

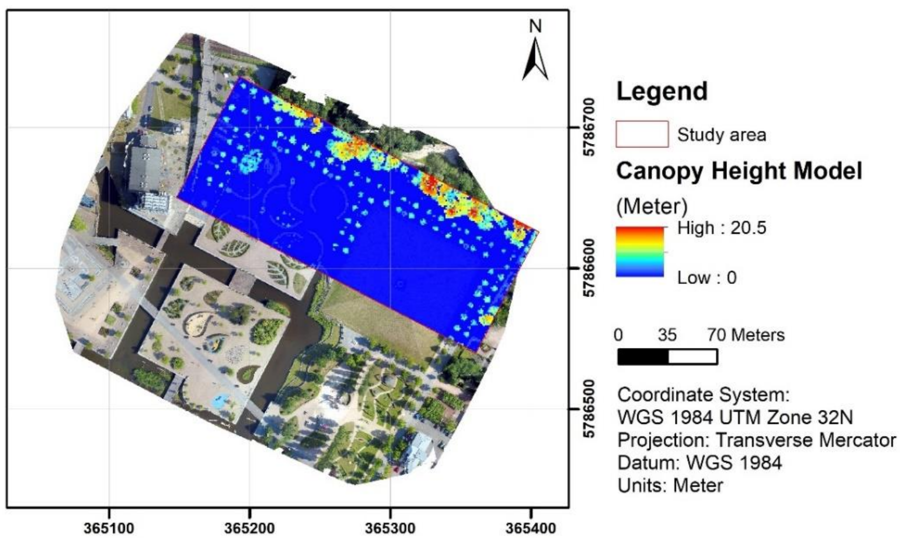

Figure 22. Canopy Height Model within the study area. The background orthophoto was acquired in July 2017 and provided by the University of Twente.

The comparison of field measured tree height, and ALS tree height is illustrated in Figure 23 below. This graph shows that the two heights are highly correlated with a 0.693 R^2 value. When $Height_{ALS}$ was used as ground truth, the root-mean-square error (RMSE) was 0.659.

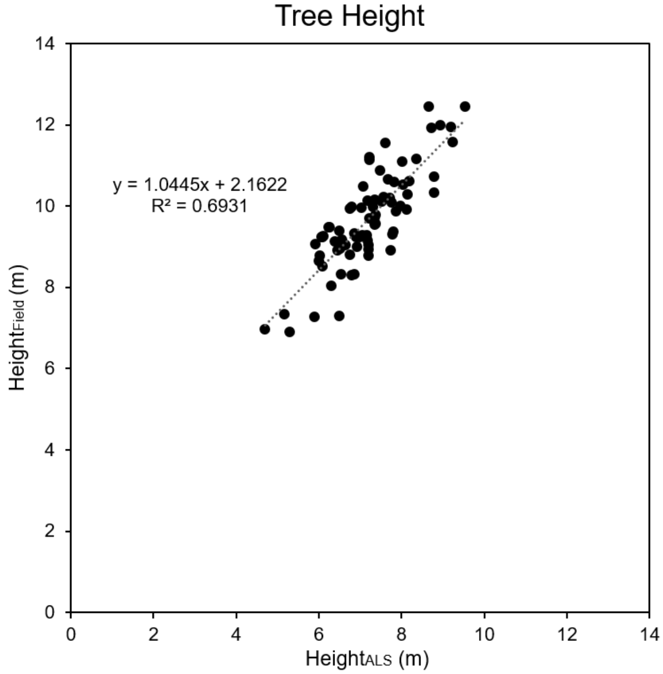

Figure 23. ALS tree height versus Laser scanner measured tree height.

3.2. Comparison of different oblique angles

Question 1 of this research is as follows: *Do oblique camera angles of UAV flights influence the point cloud density and completeness of individual tree?*

To answer this question, the oblique angles with their corresponding point cloud densities are shown in Table 9. It is indicated that the oblique camera angle influenced the density of the point cloud by comparing the quality reports generated by the Pix4D software. The point density increased considerably with the increasing oblique camera angle.

Table 9. Quality report of different oblique camera angles (leaf-on season)

Oblique camera angle	Median of matches per calibrated image	Average point density of the point cloud/m^3
35°	10352.30	97.74
40°	8606.52	252.58
45°	8220.44	474.76
50°	4375.42	862.89

However, the number of matching points and point density are not sufficient to prove that the oblique angle could influence the completeness of the main woody part of the individual tree. The point cloud is irregularly distributed since the tie-points are extracted considering the surface appearance; the points with a higher grey value contrast are easier to detect. For images acquired at 35° oblique camera angle, the median of matches per calibrated image is the largest, with a value of 10352.3; this means that feature points in an image acquired at this angle are much easier to detect. In contrast, the average point density of the point cloud in the 35° dataset is lowest, approximately 97.74 points per square metre, only approximately 1/9 of the 50° dataset. This does

not exclusively determine which oblique angle can provide the optimal point cloud for QSM. Therefore, ten individual trees for each oblique angle were extracted and used for the QSM to assess the completeness.
Figure 24 and Figure 25 below present the QSM DBHs and heights of the ten individual trees; the reference DBH and height measured in the field are also shown in the two graphs to compare with the QSM DBHs and heights of different oblique camera angles. The DBH bar chart shows that most estimated DBHs are smaller than the corresponding reference DBHs- approximately half of the reference value. For the tree height chart, notably, the QSM estimated heights of Tree002 and Tree003 are less than 5 metres, while the reference values are 2 or 3 times larger. In addition, the 35° data for Tree010 is missing in both charts because QSM cannot be successfully reconstructed. All in all, none of the QSMs can provide accurate estimates of DBH or tree height during the leaf-on season; the quality of the four datasets are too poor to support a good reconstruction of QSM with the very low completeness.

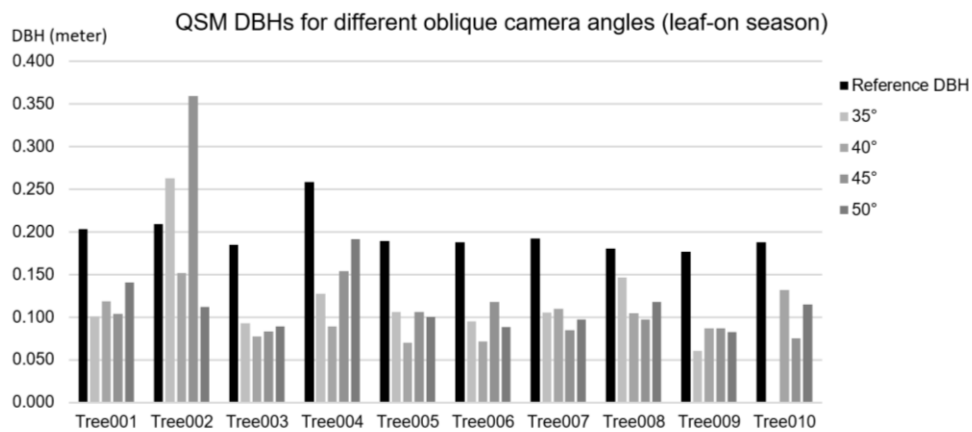

Figure 24. QSM DBHs for different oblique camera angles during the leaf-on season.

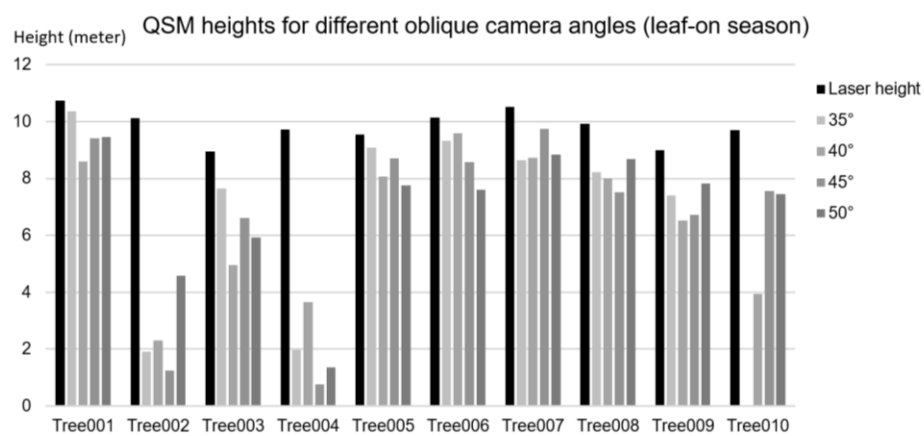

Figure 25. QSM heights compared to Laser height for different oblique camera angles during the leaf-on season.

Figure 26 illustrates the point cloud height of the ten individual trees. The individual tree point cloud cannot generate good QSM for tree parameter estimation, but it can provide an accurate estimation of tree height by measuring the distance between the lowest point and highest point.

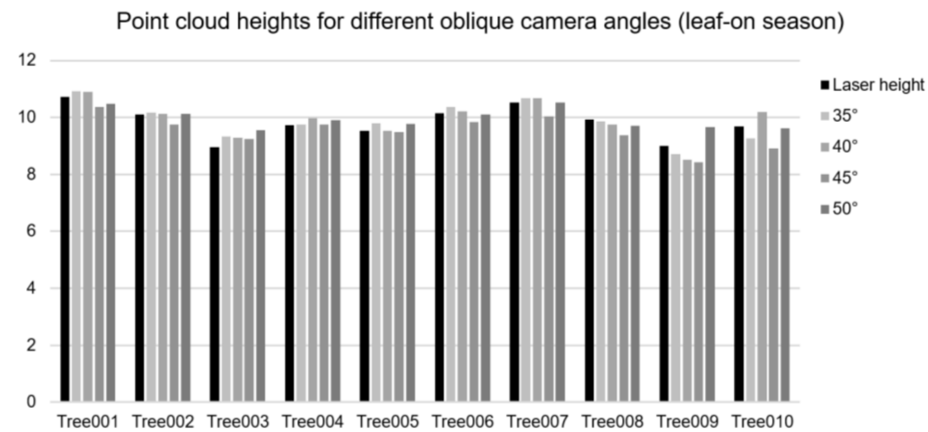

Figure 26. Point cloud heights compared to Laser height for different oblique camera angles during the leaf-on season.

Although none of the datasets is useful for the QSM, one innovative method was put forward to continue the study. Point cloud datasets of the four different camera angles were combined to increase the completeness of the individual tree. Figure 27 is an example of the combined individual tree point cloud.

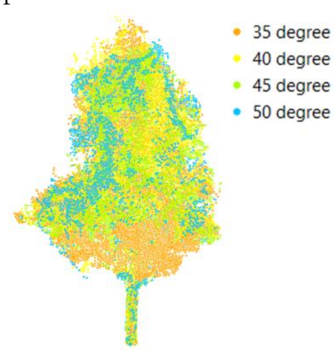

Figure 27. Combined individual tree point cloud.

Figure 28, Figure 29 and Figure30 illustrate the QSM DBH and height, point cloud height of the combined individual tree point cloud, reference DBH and height measured in the field are also shown below to compare with the estimated values. It can be observed that QSM DBHs and heights improved a lot, approximately 20% underestimation of DBH and 5% underestimation of tree height.

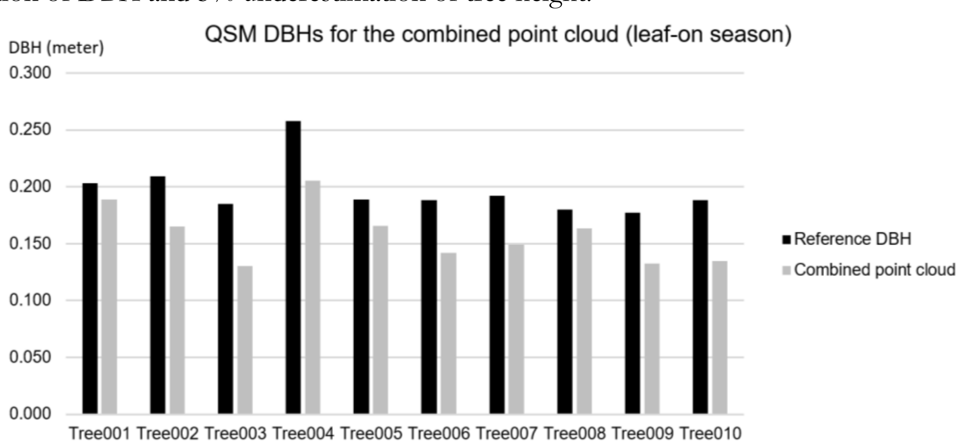

Figure 28. QSM DBHs for combined point cloud during the leaf-on season.

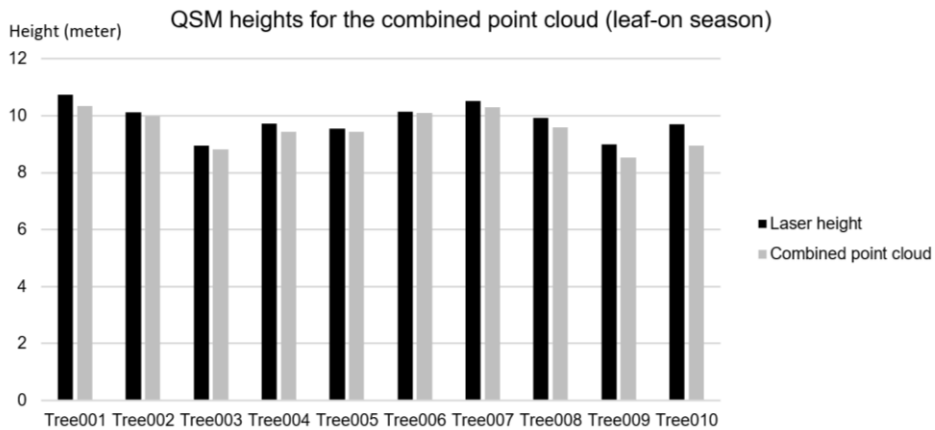

Figure 29. QSM heights for combined point cloud during the leaf-on season.

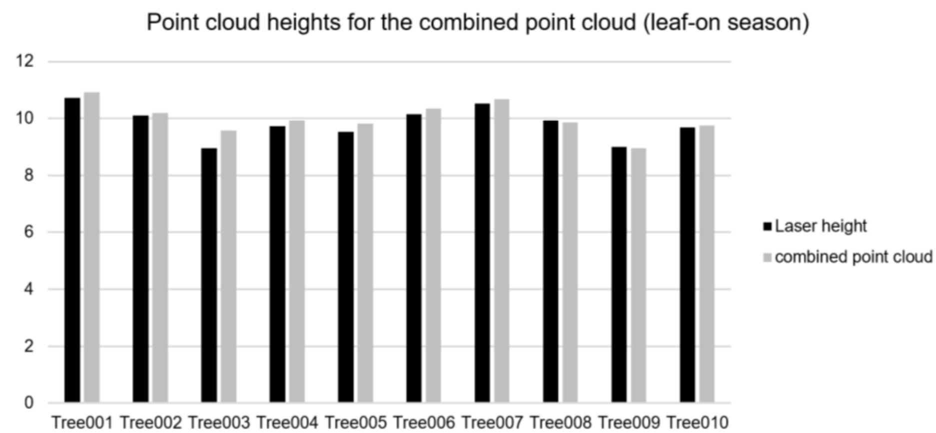

Figure 30. Point cloud heights for combined point cloud during the leaf-on season.

3.3. Estimated DBH versus reference DBH

This section answered Question 2: *Is there a significant difference between the UAV point cloud-derived DBH values, the QSM-derived DBHs, CPA-estimated DBH and the reference DBH?*

3.3.1. DBH during the leaf-on season

Figure 31 shows the comparison of field measured DBH and DBH estimated by fitting a circle around the point cloud at breast height during the leaf-on season. The best-fitted circle was estimated by minimising the distance between the circle and the points with the iterative operation. As shown in Figure 31 A1, after processing all the trees, the R^2 is quite low because of the noise points at breast height of dataset DBH_{UAV1}. Some of the noise points were noise around the stem, and some were caused by the overhanging branches at breast height which can be seen in Figure 32 (Tilon, 2017).

Hence, the noise points were manually removed by visual inspection, the DBH of some trees decreased considerably in dataset DBH_{UAV2}, and the R^2 increased dramatically, as shown in Figure 31 B1; the RMSE is 0.027. Figure 31 A2 is the DBH of a specific tree estimated with noise points, and Figure 31 B2 is the DBH of the same tree as A2 after removing the noise.

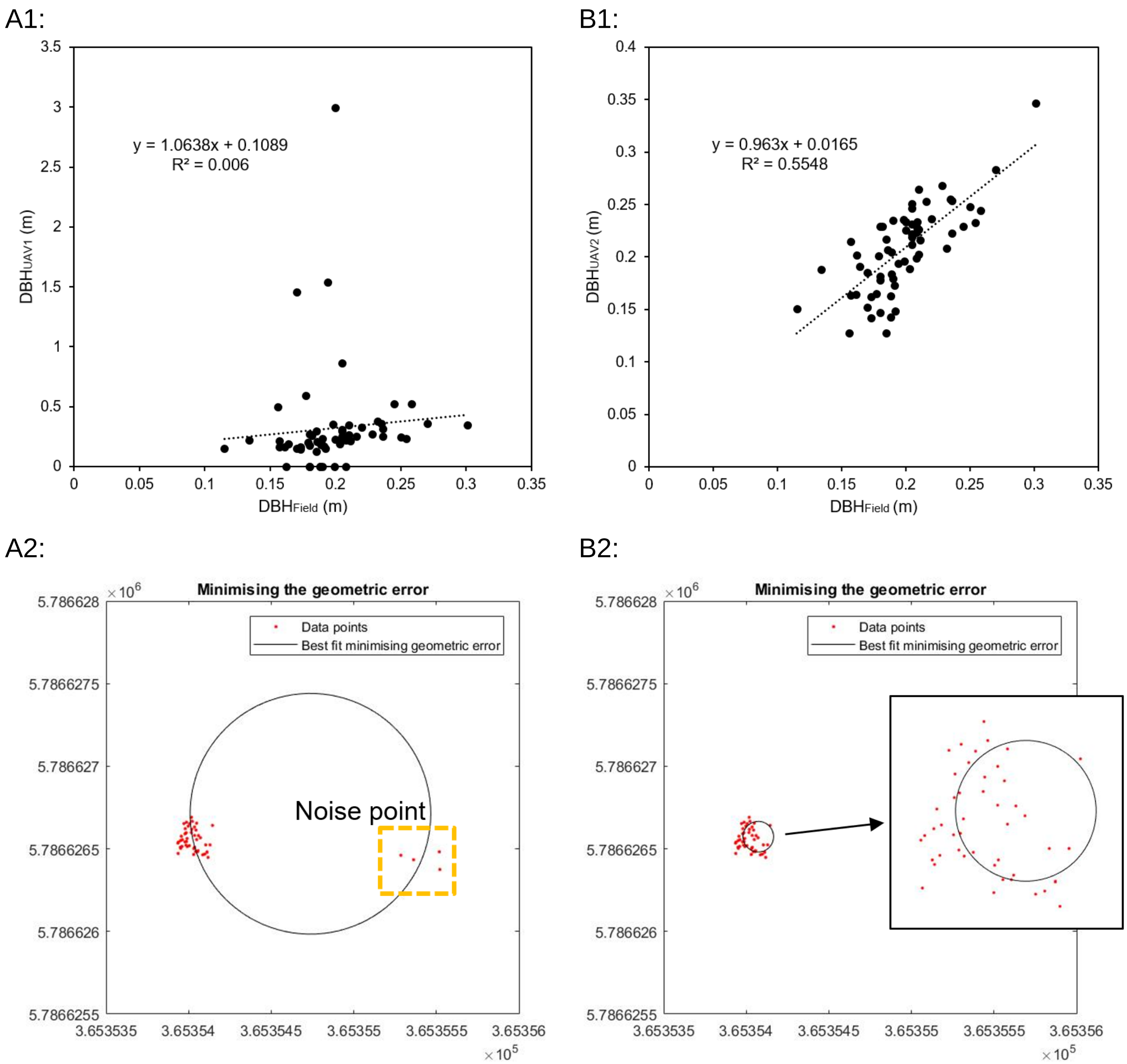

Figure 31. Reference DBH versus DBH extracted by fitting a circle around the point cloud at breast height during the leaf-on season. Image A1 is the inaccurate DBH caused by the noise at breast height which is shown in A2. Image B1 is the DBH estimates after removing the noise points. Image B2 is the new DBH after removing the noise points in Image A1.

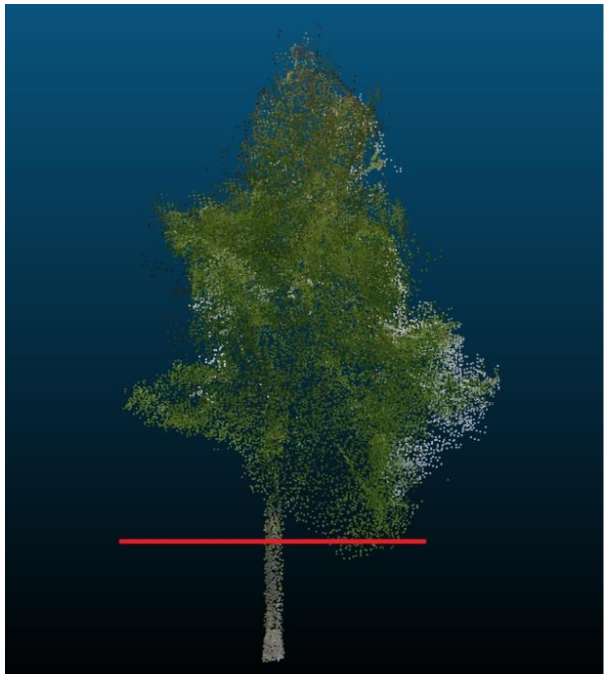

Figure 32. The outlier caused by overhanging branches. The red line indicates the breast height. The image shows that at breast height, the points of overhanging branches are also included in the slice.

Figure 33 illustrates field measured DBH versus QSM DBH (DBH_{QSM} and DBH_{CYL}) estimates during the leaf-on season. The DBH_{QSM} is extracted from the QSM cylinder at 1.3 m height, while DBH_{CYL} is the diameter of the cylinder fitted to the points between 1.1 and 1.5 m (Raumonen, 2017). The RMSE of DBH_{QSM} versus DBH_{Field} is 0.031, and the RMSE of DBH_{CYL} versus DBH_{Field} is 0.032.

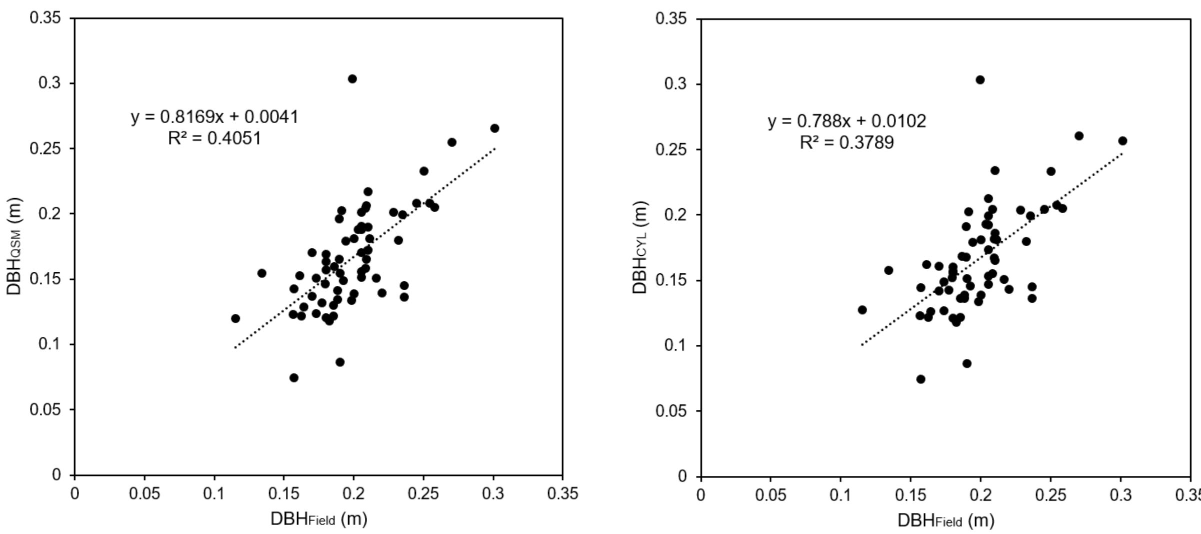

Figure 33. Field measured DBH versus DBHs extracted by QSM during the leaf-on season.

3.3.2. DBH during the leaf-off season

Figure 34 compares the reference DBH with DBH extracted by fitting a circle around the point cloud at breast height during the leaf-off season. The point cloud at breast height also has noise points, similar to those during the leaf-on season (Figure 32). An extra noise removal process was performed to obtain more accurate DBH value (Figure 34 B), and the RMSE of DBH_{UAV2} versus DBH_{Field} is 0.024.

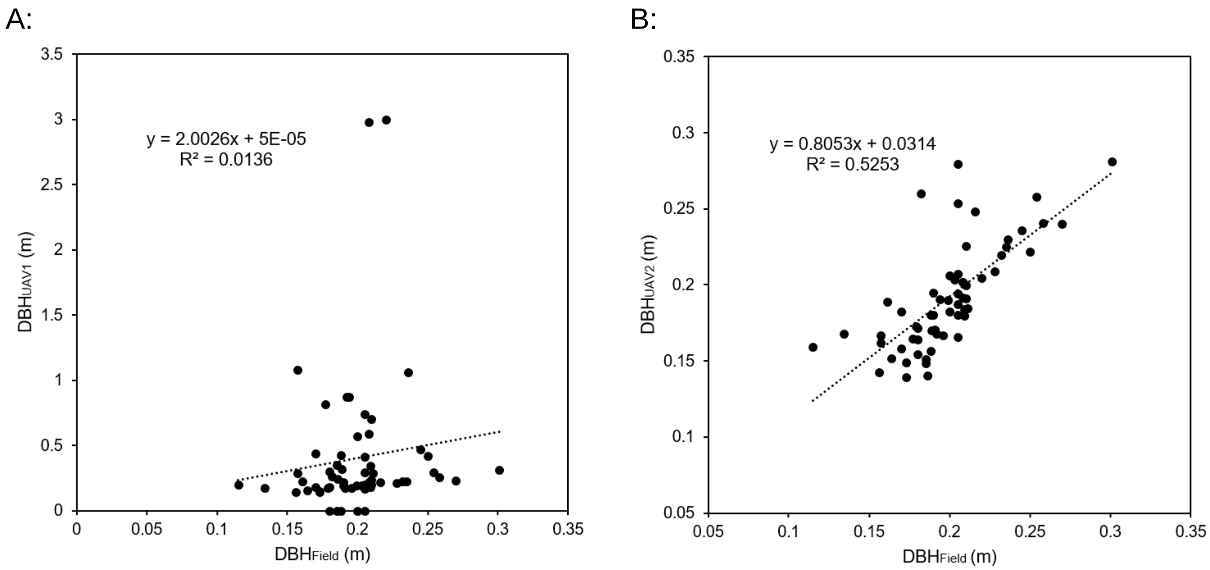

Figure 34. Reference DBH versus DBH extracted by fitting a circle around the point cloud at breast height during the leaf-off season. Image A is the result before removing the noise point; image B is the result of removing the noise points.

Figure 35 provides comparisons of two QSM DBH datasets (DBH_{QSM} and DBH_{CYL}) and the reference dataset. The red dots are noise and should be removed. The criteria for defining noise will be explained next.

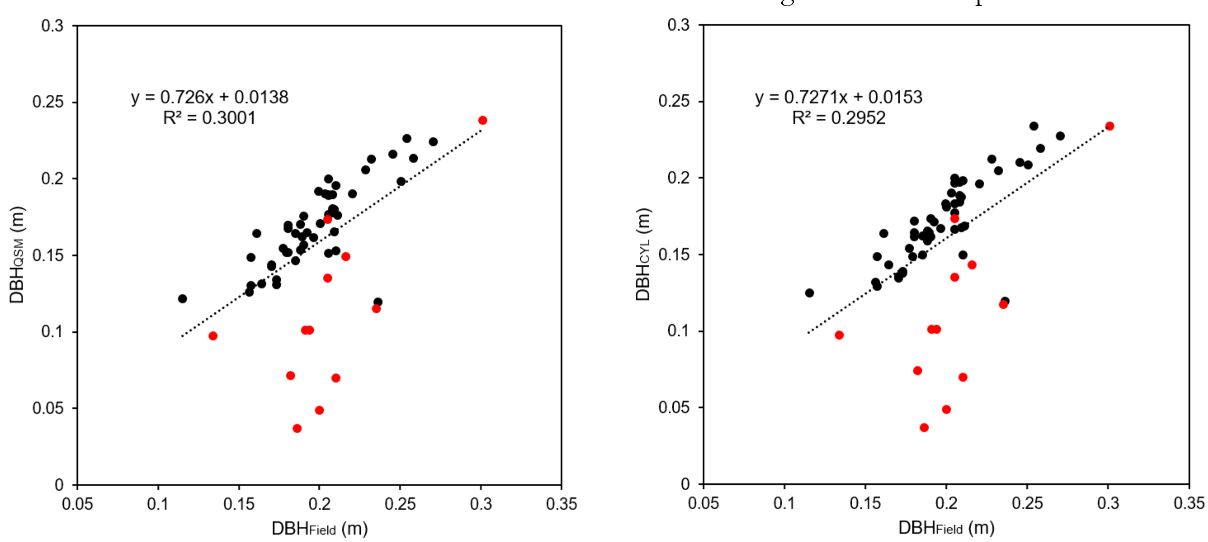

Figure 35. Field measured DBH versus DBHs extracted by QSM during the leaf-off season. The red dots are defined as outliers.

As mentioned in the methodology section 2.4.1, the individual tree point cloud should be filtered before the QSM reconstruction. However, there is not only one parameter set that applies to all trees. Some trees keep the complete structure of the woody parts after filtering, such as Tree A in Figure 36, while some become fragmented which can increase the uncertainty of the reconstruction, such as the Tree B in Figure 36. By checking the DBH values and the corresponding filtering information— the percentage of remaining points of individual trees after the filtering process (Annex Figure 1), almost all the extreme DBH values appeared when the percentage of remaining points was lower than 45%. The tree structure is imperfect when too many points are removed, and in this case, 45% is the threshold. As a result, the DBH estimates under the 45% threshold were removed from the dataset.

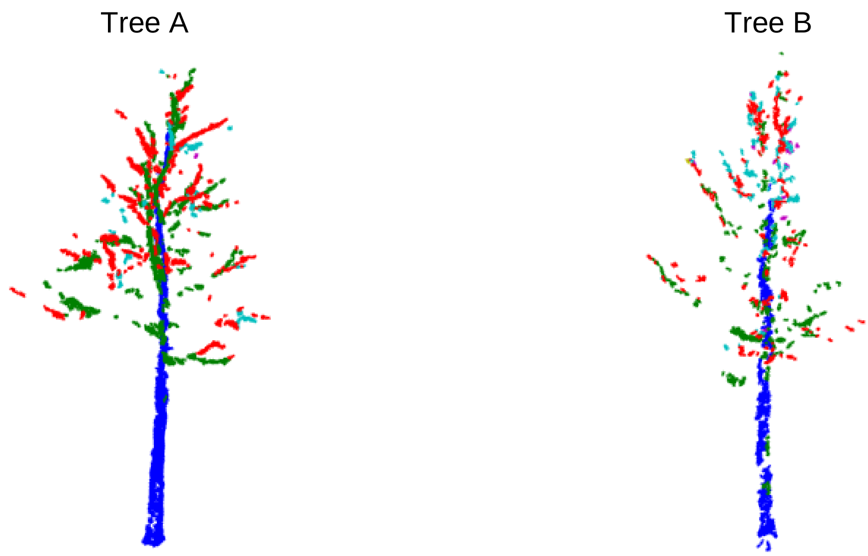

Figure 36. The individual tree point cloud after filtering. Tree A keeps the complete structure of the woody parts after filtering; Tree B is fragmented after the filtering process.

Figure 37 is the summary of the filtering information. Estimated DBH values of 12 trees out of the 61 samples were defined as outliers and were removed in this study.

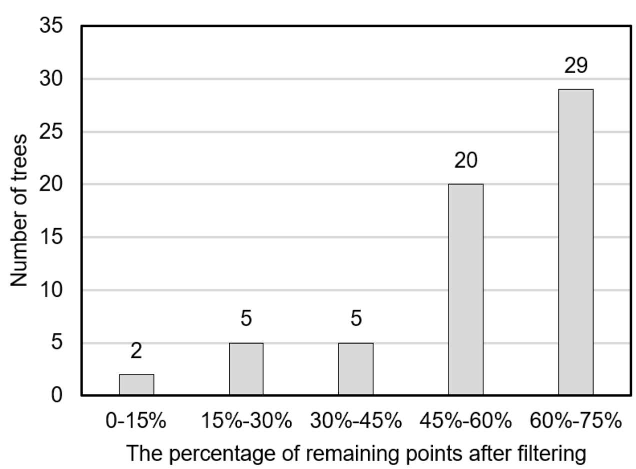

Figure 37. The percentage of remaining points after the filtering process during the leaf-off season.

Figure 38 illustrates the field measured DBH versus DBH values extracted by QSM after removing outliers in leaf-off season. The RMSE of DBH_{QSM} versus DBH_{Field} is 0.017, and the RMSE of DBH_{CYL} versus DBH_{Field} is 0.017.

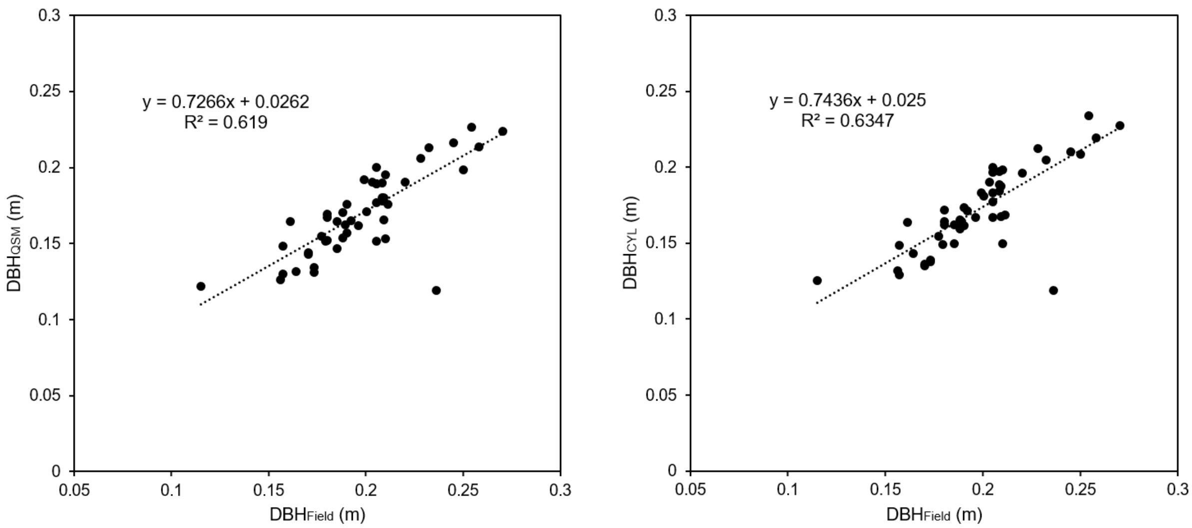

Figure 38. Field measured DBH versus DBH values extracted by QSM after removing outliers during the leaf-off season.

3.3.3. DBH estimated by CPA

Figure 39 shows the scatter plot for CPAs (CPA_{UAV} and CPA_{otho}) and DBH_{Field}. A linear regression was used to fit the model of CPA and DBH. 60% of the dataset was randomly selected to fit the model and remaining 40% of the dataset was used for validation.

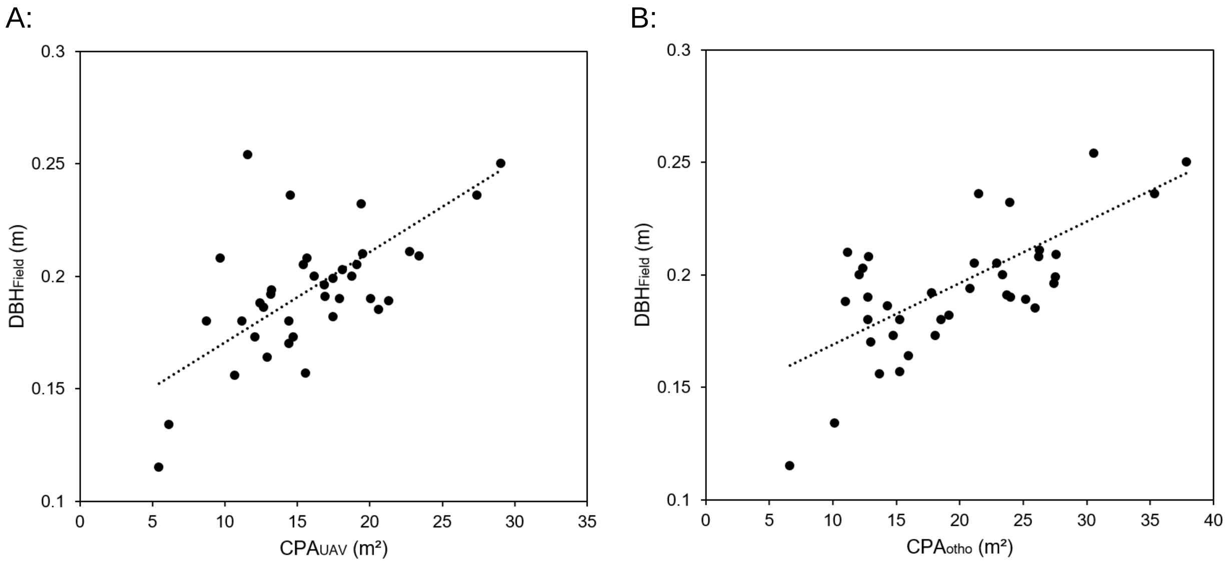

Figure 39. Scatter plot of CPAs with field measured DBH during the leaf-on season. The CPA_{UAV} in image A is generated by point cloud rasterization; the CPA_{otho} in image B is extracted from orthophoto.

Table 10 illustrates the regression models for the relationship of CPA and DBH, the calibration and validation results are also included in the table.

Table 10. Regression models with calibration and validation statistics for CPA and DBH

Regression models	Constants		Calibration(n=39)	Validation (n=26)	
	a	b	R^2	RMSE	RMSE%
$DBH=a+b*CPA_{UAV}$	0.1305	0.0040	0.4120	0.017	8.54
$DBH=a+b*CPA_{otho}$	0.1415	0.0027	0.3659	0.019	9.53

3.4. Estimated tree height versus reference tree height

This section answered Question 3: *Is there a significant difference between the UAV point cloud-derived height values, the QSM-derived heights and the reference heights?*

3.4.1. Tree height during the leaf-on season

Figure 40 illustrates the comparison of reference heights and estimated height, which is the vertical distance from the lowest point to the highest point of the individual tree point cloud. As shown in Figure 40, the R^2 of graph B is smaller than that of graph A, with different explanatory variables ($Height_{Field}$ for A and $Height_{ALS}$ for B) and the same response variable. The RMSE of $Height_{Field}$ versus $Height_{UAV}$ is 0.559, and the RMSE of $Height_{ALS}$ versus $Height_{UAV}$ is 0.749.

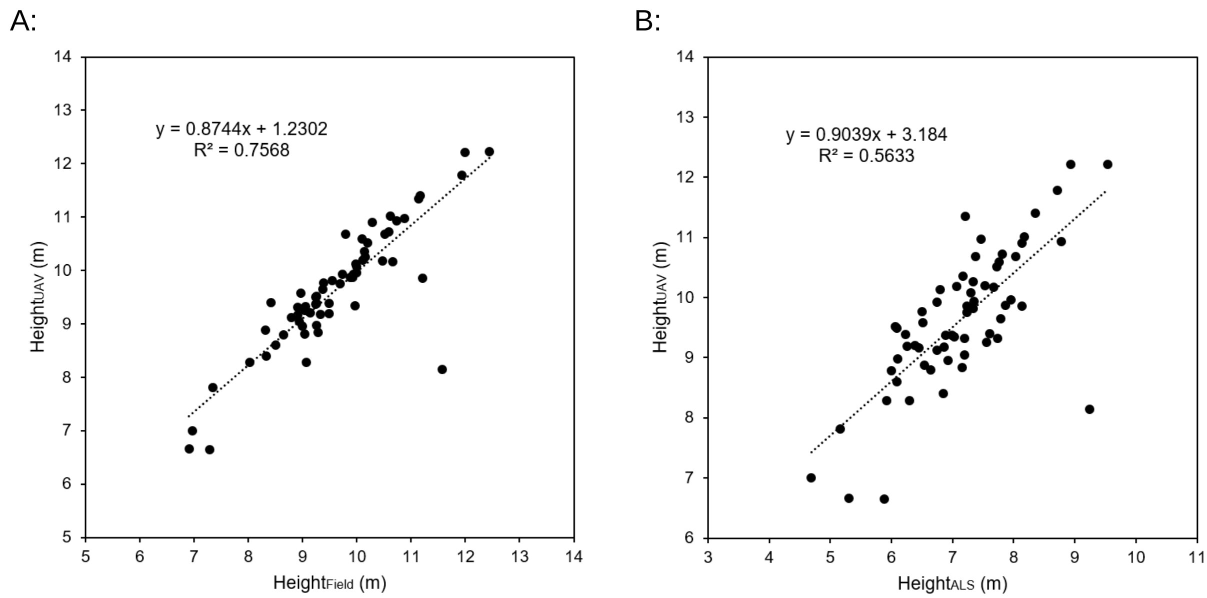

Figure 40. Reference heights versus height extracted from point cloud during the leaf-on season. In graph A, $Height_{Field}$ is used as the explanatory variable. In graph B, $Height_{ALS}$ is explanatory variable.

Figure 41 shows the correlations between reference heights and the QSM estimated height. The red dots are defined as outliers and were not included in the analysis.

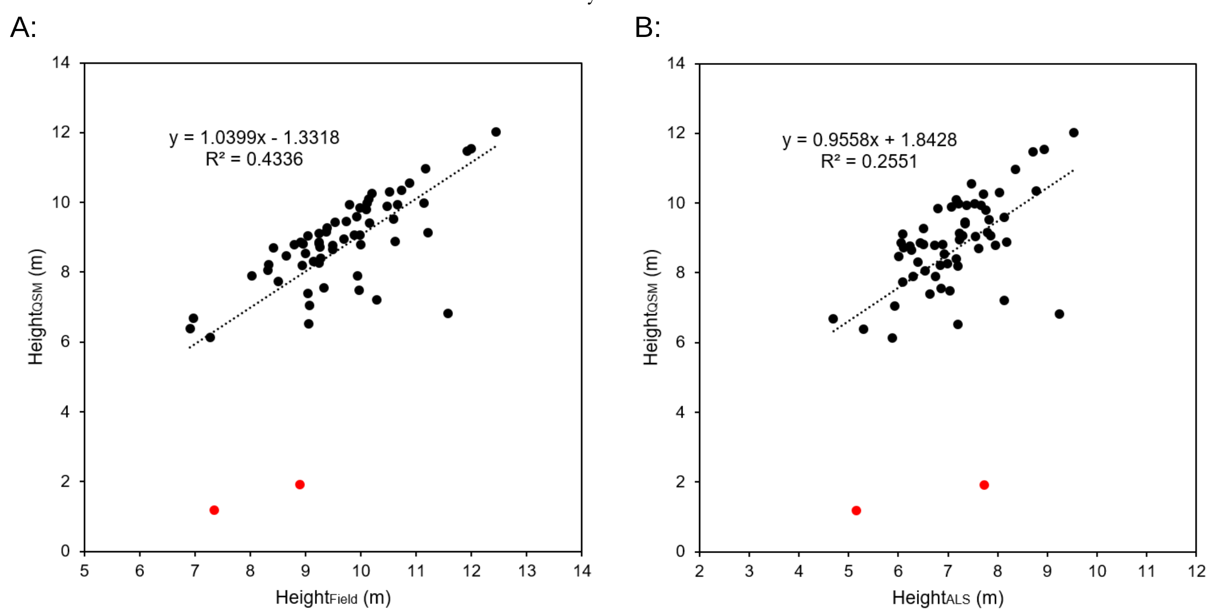

Figure 41. Reference heights versus QSM height during the leaf-on season. The red dots are defined as outliers.

The filtering process can have a tremendous influence on the QSM result; this process removes the noise points, which is kind of a basis for correct QSM reconstruction. However, for point clouds acquired during the leaf-on season, removing noise points is an awkward question. The points at the canopy part are leaves in reality, and the large canopy occludes the top trunk part. As a result, only the lower trunk part is left after the filtering process (Figure 42), and the tree height estimated by QSM can be extremely small in this situation, which is then recognised as an outlier.

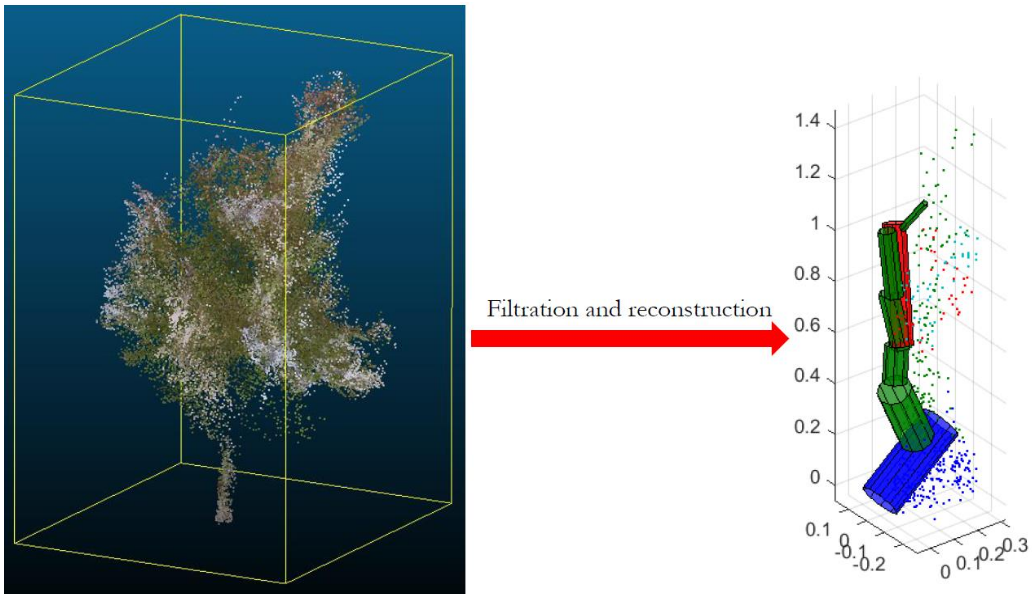

Figure 42. The source of the outlier in QSM tree height estimation. The canopy part is removed after the filtering process; as a result, the QSM is incomplete.

Figure 43 is the result after removing the two outliers and the values of R^2 for both increase considerably, the RMSE of $Height_{Field}$ versus $Height_{QSM}$ is 0.857, and the RMSE of $Height_{ALS}$ versus $Height_{QSM}$ is 0.993.

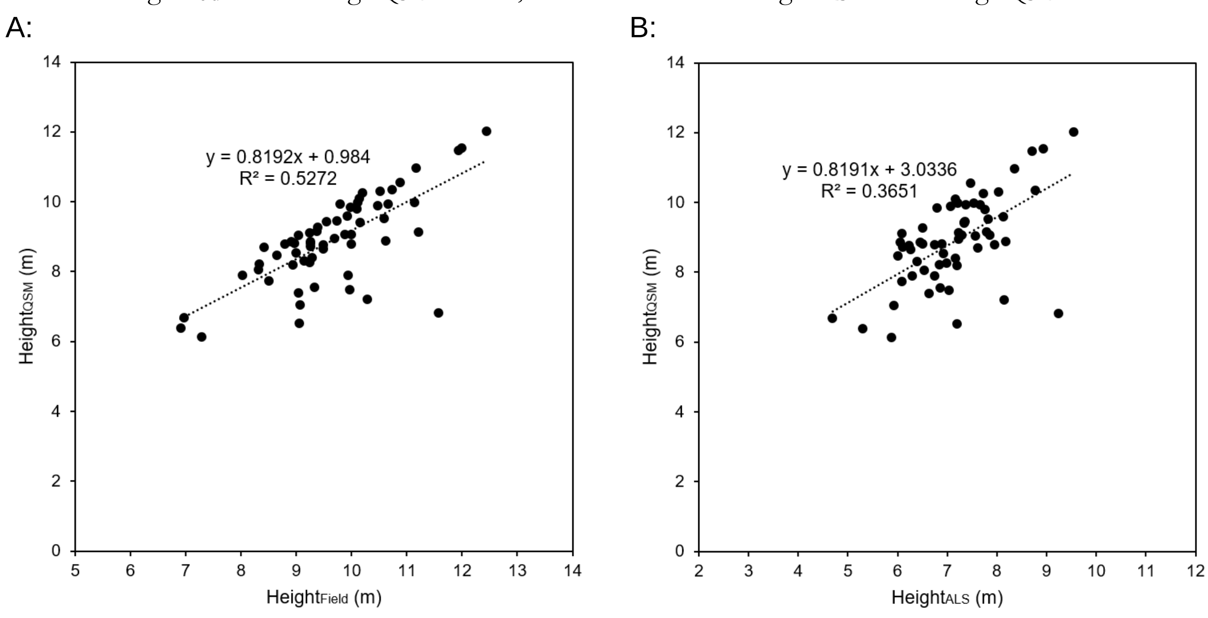

Figure 43. Reference heights versus QSM height after removing outliers during the leaf-on season.

3.4.2. Height in leaf-off season

The tree height measured using the UAV generated point cloud is plotted against the reference heights, shown in Figure 44. The regression equation and R^2 value are also shown in the plot chart; the RMSE of $Height_{Field}$ versus $Height_{UAV}$ is 0.643, and the RMSE of $Height_{ALS}$ versus $Height_{UAV}$ is 0.730. It is clear that the height extracted from the point cloud is lower than the reference height since the acquisition time of this dataset was during the leaf-off season.

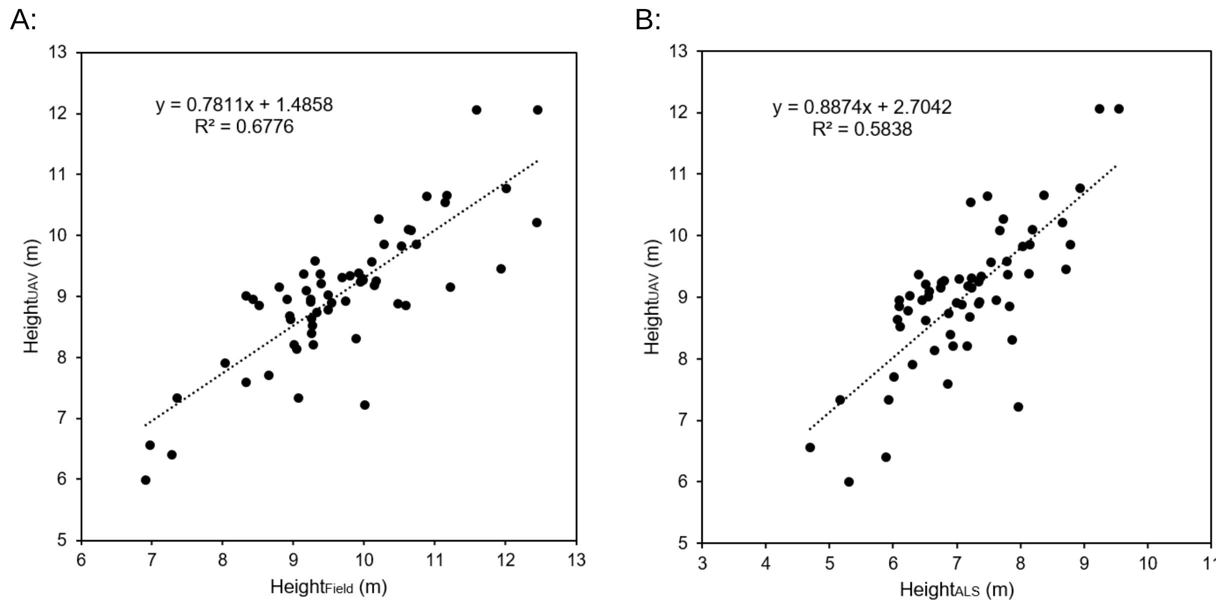

Figure 44. Reference heights versus height extracted from individual tree point clouds during the leaf-off season.

The tree height estimated by QSM is plotted against the reference heights, as shown in Figure 45. The regression equation and R^2 are also shown in the image; the RMSE of $Height_{Field}$ versus $Height_{QSM}$ is 0.768, and the RMSE of $Height_{QSM}$ versus $Height_{UAV}$ is 0.902.

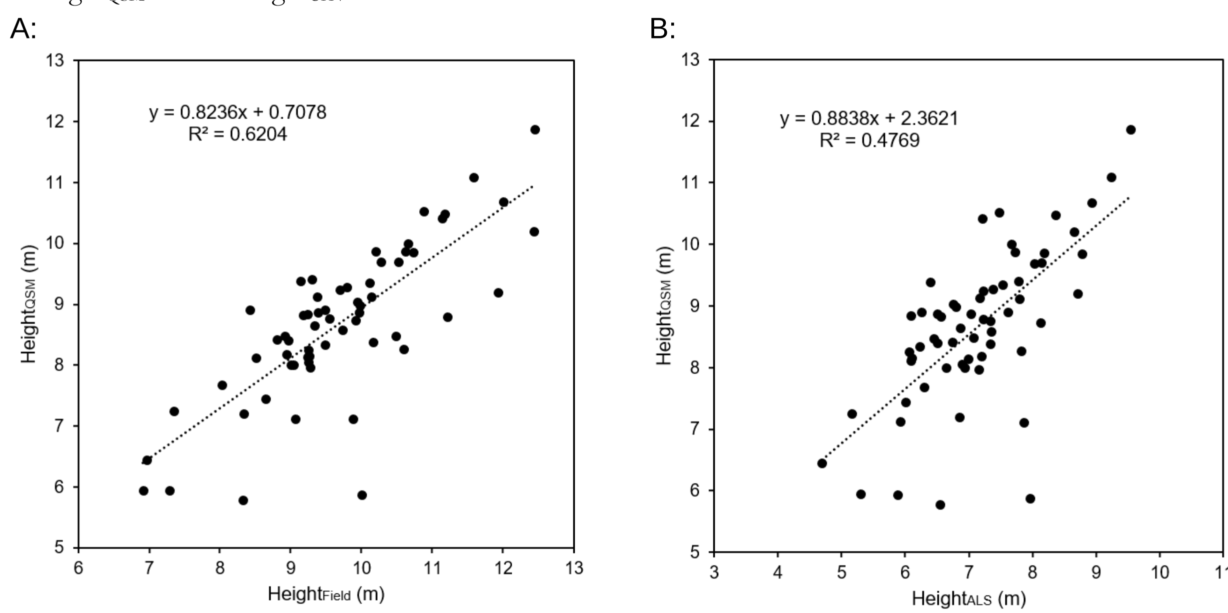

Figure 45. Reference heights versus QSM height during the leaf-off season.

3.5. Summary of the independent t-test for DBH and height

A two-sample t-test was conducted on the estimated DBH and reference DBH datasets and the estimated heights and reference heights to determine whether there is a difference between the means between the mean values. The null hypothesis states that there is no difference between the mean values, while the alternative hypothesis states that there is a significant difference between the mean values. The H_0 hypothesis is rejected on a 95% confidence interval ($\alpha = 0.05$).

Table 11 shows the results of the independent sample t-test for DBHs. By checking the corresponding p-value, DBH_{QSM} and DBH_{CYL} both show a significant difference between the mean values compared to DBH_{Field}, while no significant difference is found for DBH_{UAV2}[1] compared to DBH_{Field}.

Table 11. Result of the two-sample t-test comparing DBH_{Field} and estimated DBHs

	Statistic	DBH_{UAV2}	DBH_{QSM}	DBH_{CYL}	DBH_{CPA1}	DBH_{CPA2}
Leaf-on season	H_0 accepted	**Yes**	No	No	**Yes**	**Yes**
	n	**63**	63	63	**65**	**65**
	P-value	**0.089250**	0.000003	0.000004	**0.863263**	**0.742955**
Leaf-off season	H_0 accepted	**Yes**	No	No	-	-
	n	**61**	49	49	-	-
	P-value	**0.367649**	0.000002	0.000012	-	-

Table 12 and 13 show the results of the independent sample t-test for tree heights. By checking the corresponding p-value, only $Height_{UAV}$ for the leaf-on season shows there is no significant difference with the Laser scanner measured tree height ($Height_{Field}$).

Table 12. Result of two-sample t-test comparing $Height_{ALS}$ and estimated heights

	Statistic	$Height_{UAV}$	$Height_{QSM}$
Leaf-on season	H_0 accepted	No	No
	n	63	61
	P-value	1.587E-27	1.569E-15
Leaf-off season	H_0 accepted	No	No
	n	61	61
	P-value	1.144E-18	1.566E-12

Table 13. Result of two-sample t-test comparing $Height_{Field}$ and estimated heights

	Statistic	$Height_{UAV}$	$Height_{QSM}$
Leaf-on season	H_0 accepted	**Yes**	No
	n	**63**	61
	P-value	**0.838014**	0.000318
Leaf-off season	H_0 accepted	No	No
	n	61	61
	P-value	0.001787	0.000004

[1] DBH_{UAV2} is the DBH extracted by fitting a circle around the UAV point cloud after removing the noise point.

3.6. Assessment of biomass estimated by different methods

This section answered Question 4: *Is there a significant difference between the AGB calculated by the QSM volume, the AGB calculated by allometry using DBH (estimated by CPA) and UAV-point cloud height as input, the AGB calculated by point cloud-derived DBH and height, the AGB derived from allometry that uses QSM-derived DBH and height, and the AGBs calculated by allometry that use reference DBH and height as input?*

3.6.1. Trunk biomass calculated by allometric equation in leaf-on season

For the leaf-on season, QSM was generated using the combined point cloud as input. However, there is a serious problem caused by the leaves. The sunlight cannot penetrate the non-transparent object; consequently, the branch cannot be recorded due to the foliage shield, and most points at the canopy part are useless for the reconstruction of woody parts. Also, the noise point at the canopy part cannot be removed entirely. If the parameters of the filtering are too low, the points of the trunk part will also be removed; then, the QSM cannot generated a whole tree (Figure 46 A). When the parameters are increased, the QSM is generated, but at the canopy part, the branch volume is overestimated (Figure 46 B).

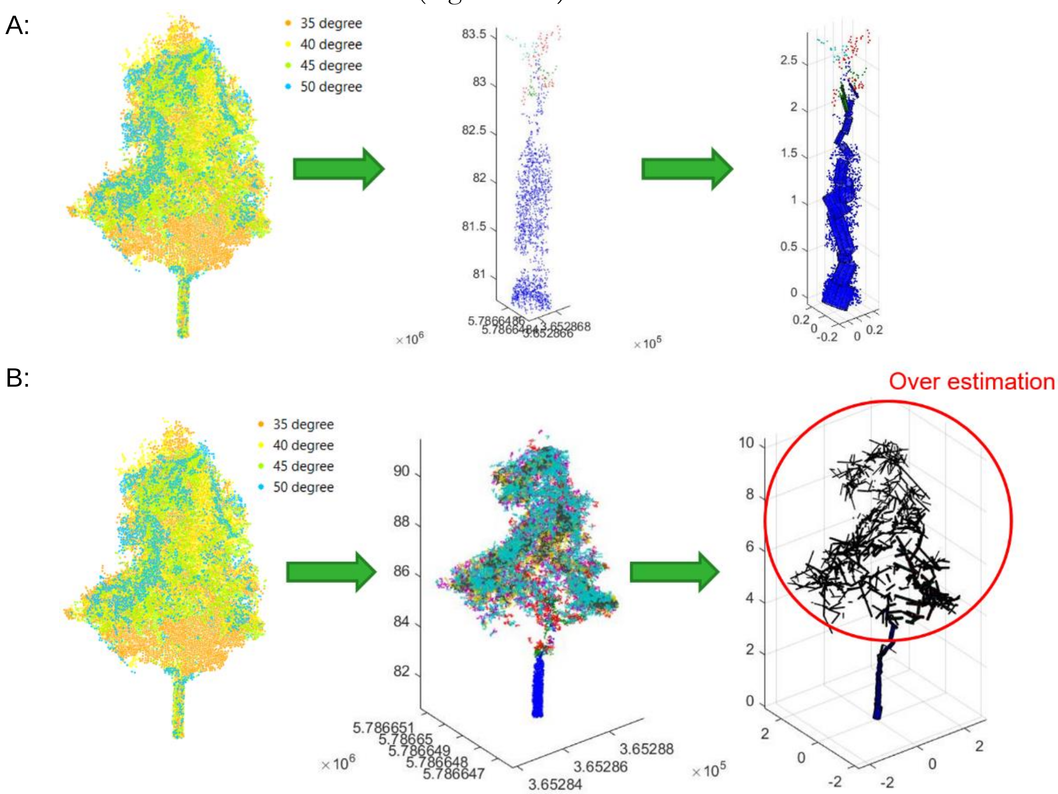

Figure 46. The influence of filtering for biomass estimation. Image A illustrates the QSM with low filtering parameters, and Image B is the QSM of high filtering parameters.

The QSM based *TotalVolume*, *TrunkVolume* and *BranchVoulme* could be directly used for biomass estimation without the allometric equation, but the *TotalVolume* and *BranchVoulme* showed overestimation in leaf-on season. Thus, only *TrunkVolume* was used for the accuracy assessment. In addition, the allometric equation developed for trunk volume was used for biomass calculation for the leaf-on season. Even so, the trunk biomass calculated with *TrunkVolume* leads to underestimation, because the trunk structure of the tree was not recorded by UAV images at the canopy part in QSM, while the trunk volume based allometric equation included the trunk from the ground line to the 5-cm top.

3.6.2. AGB calculated by the allometric equation for the leaf-off season

For the leaf-off season, the QSM of individual trees could be reconstructed without the occlusion problem (Figure 47). Thus, the *TotalVolume* was used for the biomass calculation. In addition, the allometric equation for total biomass estimation was used for the leaf-on season.

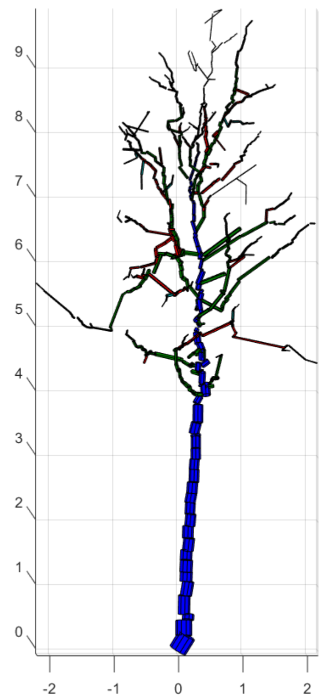

Figure 47. The QSM for the leaf-off season.

3.6.3. Summary

Table 14 shows the mean and standard deviation of biomass calculated by QSM and through tree allometry. It heights that the mean of AGB_{QSM} is lower than AGBs calculated by tree allometry.

Table 14. Statistics of biomass estimations derived from QSM and through tree allometry

		AGB_{QSM}[2]	$Allo_{QSM}$[3]	$Allo_{UAV}$[4]	$Allo_{Field1}$[5]	$Allo_{Field2}$[6]	$Allo_{CPA1}$[7]	$Allo_{CPA2}$[8]
Leaf-on season trunk biomass (n=61)	SD	19.173	24.176	33.272	20.057	26.401	17.776	15.429
	Mean	34.410	43.479	69.481	47.500	63.581	60.783	59.564
Leaf-off season AGB (n=49)	SD	27.270	33.359	44.435	36.964	46.915	31.536	31.516
	Mean	72.890	85.226	105.345	92.278	124.005	115.303	113.913

Table 15 is the summary of the correlation between AGB_{QSM} and biomass estimated through tree allometry.

Table 15. The correlation between biomass estimated by QSM and through tree allometry

	Statistic	$Allo_{QSM}$	$Allo_{UAV}$	$Allo_{Field1}$	$Allo_{Field2}$	$Allo_{CPA1}$	$Allo_{CPA2}$
Leaf-on season	Correlation coefficient	1.102	1.321	0.860	1.117	0.596	0.495
trunk biomass	intercept	5.556	24.027	17.898	25.144	40.281	42.547
n=61	R square	0.764	0.579	0.676	0.658	0.413	0.378
Leaf-off season	Correlation coefficient	0.975	1. 003	0.978	1.277	0.744	0.810
AGB	intercept	14.160	32.228	21.012	30.942	61.086	54.888
n=49	R square	0.635	0.379	0.520	0.551	0.414	0.491

The summary of paired t-tests of AGB estimated by QSM, and AGB calculated through tree allometry is shown in Table 16. Significant differences exist between AGB_{QSM} and other AGB estimates no matter in leaf-on season or not. Table 17 shows the model accuracy by calculating the overestimation/underestimation rate.

Table 16. Results of pairwise t-tests for AGB estimates derived from QSM and through tree allometry

	Statistic	$Allo_{QSM}$	$Allo_{UAV}$	$Allo_{Field1}$	$Allo_{Field2}$	$Allo_{CPA1}$	$Allo_{CPA2}$
Leaf-on season	H_0 accepted	No	No	No	No	No	No
trunk biomass	T test	-5.948	-12.208	-8.720	-14.603	-13.144	-12.628
n=61	P-value	1.499E-7	6.602E-18	2.924E-12	2.043E-21	2.571E-19	1.520E-18
Leaf-off season	H0 accepted	No	No	No	No	No	No
AGB	T test	-4.283	-6.488	-5.299	-11.065	-11.811	-12.443
n=49	P-value	0.000088	4.493E-8	0.000003	8.328E-15	8.283E-16	1.240E-16

Table 17. The over-/underestimation of different methods comparing with reference dataset ($Allo_{Field2}$)

	AGB_{QSM}	$Allo_{QSM}$	$Allo_{UAV}$	$Allo_{Field1}$	$Allo_{CPA1}$	$Allo_{CPA2}$
Leaf-on season trunk biomass (n=61)	-45.88%	-31.62%	9.28%	-25.29%	-4.40%	-6.32%
Leaf-off season AGB (n=49)	-43.26%	-17.09%	-27.63%	-33.31%	-9.06%	-10.18%

[2] $AGB_{QSM} = Volume_{QSM} \times$ wood density
[3] $Allo_{QSM}$=Allometry (DBH_{QSM}, $Height_{QSM}$)
[4] $Allo_{UAV}$=Allometry (DBH_{UAV}, $Height_{UAV}$)
[5] $Allo_{Field1}$=Allometry (DBH_{Field}, $Height_{ALS}$)
[6] $Allo_{Field2}$=Allometry (DBH_{Field}, $Height_{Field}$)
[7] $Allo_{CPA1}$=Allometry (DBH_{CPA1}, $Height_{UAV}$)
[8] $Allo_{CPA2}$=Allometry (DBH_{CPA2}, $Height_{UAV}$)

4. DISCUSSION

4.1. Reference data acquisition

During the DBH collection, the diameter tape was wound around the trunk in the horizontal plane at breast height. Köhl, Magnussen, & Marchetti (2006) stated that bias could be produced during the measurements for the following reasons: positive bias caused by noncircular cross section; instrumental error caused by stretching of cloth/fibreglass tapes; and operator error caused by an incorrect location of breast height. During the filed measurements, the breast height was determined using a marked T-shirt (Figure 48), which was prone to get an incorrect location of breast height. It's undoubtedly that bias happened during the field measurements, but the error of filed measured DBH was out of the scope of this study.

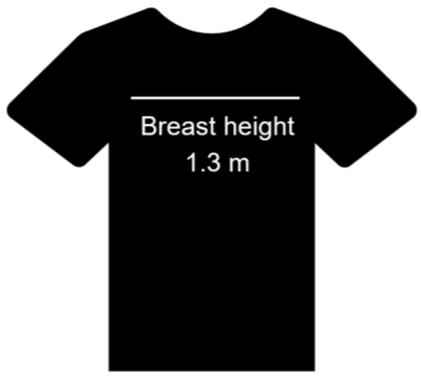

Figure 48. T-shirt used for DBH measurement.

There is a difference between the $Height_{ALS}$ and $Height_{Field}$. This is also highlighted by the high error (RMSE)-0.659 m observed when $Height_{ALS}$ is used as an independent variable, and the laser measured $Height_{Field}$ as a dependent variable, where the correlation coefficient is 1.0445 with a constant of 2.1622.

During the field data collection, $Height_{Field}$ was measured with a laser scanner- Leica Disto™ D510. Errors appeared when it was difficult to identify the top of the tree (Figure 49 A), or the tree was not perpendicular to the ground (swung with the wind in this case) (Figure 49 B); this fact was also mentioned by Dassot, Constant, & Fournier (2011) and Hopkinson, Chasmer, Young-Pow, & Treitz (2004).

A: B:

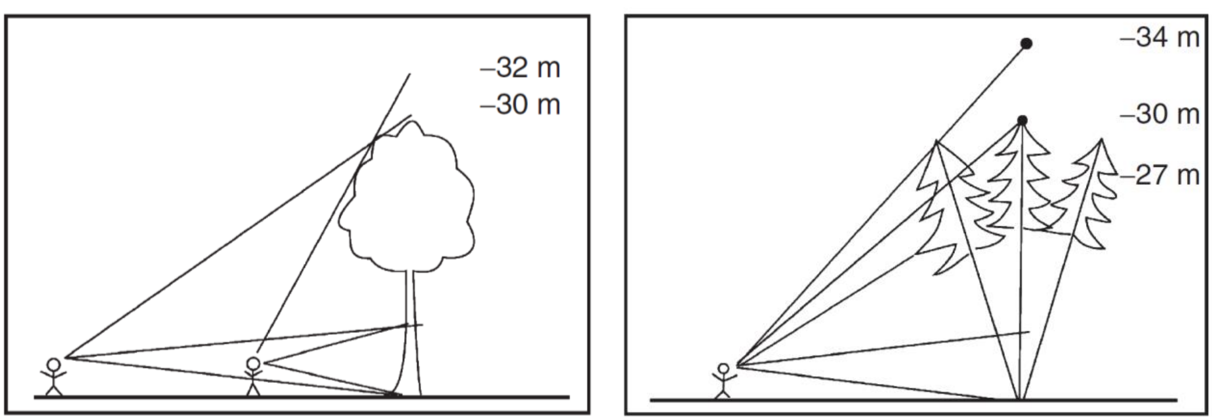

Figure 49. Sources of errors in height measurements (Paul Schmid-Haas, Ernst Baumann, 1978. as cited in Köhl, Magnussen, & Marchetti, 2006).

For the ALS, the laser pulse is able to penetrate the canopy, which will result in the underestimation of tree height. Mehtätalo, Virolainen, Tuomela, & Packalen (2015) explained the reasons for penetration as follows: 1) the pulse hit the gap between the branches of the crown and 2) energy is accumulated to generate detectable reflected echoes for the sensor. In addition, negative height bias occurred with $\text{Height}_{\text{ALS}}$ because of the growing season when compared with the $\text{Height}_{\text{Field}}$ (Mehtätalo et al., 2015), since the ALS data were acquired before the growing season in early 2017, while the field data collection was carried out after the growing season in 2017. The annual tree growth could account for 0.6-0.9 m difference (Johnson, 1985), so the field-measured tree height during the leaf-on season will be used as for the reference AGB calculation.

4.2. UAV data acquisition and SfM

Compared with the data collection of TLS, UAV image acquisition was more convenient and faster. The UAV worked well with the linear-shaped study area, and there is no need to move heavy instruments from time to time as with TLS. In practice, the most time-consuming parts of UAV data collection were making the flight plan and the selection and collection of GCPs. However, for the TLS data collection, the scan position should be planned beforehand, and the GCPs and reflectors all need to be appropriately located; these first-phase preparations can require considerable time as well.

Despite the aforementioned benefits, there were some unexpected circumstances that occurred during the UAV flight, such as changing sunlight and high wind speed, which negatively influenced the data processing and the quality of the final products.

4.2.1. Problems caused by sunlight and wind

The change in sunlight during a flight resulted in poor-quality images. The cloudy weather decreased the radiometric quality of the images, and the camera could not modify itself automatically to the change in sunlight intensity. As a result, underexposed and overexposed images were collected (Figure 50), and those images negatively affected the SfM process together with the accuracy and density of the generated point clouds and orthophoto (Wierzbicki, Kedzierski, & Fryskowska, 2015).

Figure 50. The underexposed and overexposed images caused by the changing sunlight during one flight.

Wind speed directly affects the stillness of the shots. Figure 51 illustrates the blurred image collected on a windy day; during the flight, the wind speed exceeded 9 metres per second—the pilot suggested a safety threshold. This was mainly creating problems during the leaf-on season.

Figure 51. Comparison of a blurred image and normal image during the 35° oblique angle flight on 4th October 2017.

A blurred image has a significant influence on the SfM. Sieberth, Wackrow, & Chandler (2015) listed the facts of blurred image generation as follows: wind and turbulence during the UAV flights, sudden input by the operator and the flight movement of the drone, and the vibrations of the engines. In our case, the main factor was the wind. The first step of SfM is to detect feature points and find corresponding feature points in multiple images. However, the same feature points can appear differently in the images due to the blur. Consequently, matching corresponding points becomes increasingly difficult, errors occur, and accuracy decreases (Sieberth, Wackrow, & Chandler, 2014). In this study, SfM was automatically processed in Pix4D, the problem caused by blurred image was not studied. Lee & Lee (2013) proposed a blur-aware depth reconstruction method to handle the problem caused by blurred, Sun, Cao, Xu, & Ponce (2015) using a Convolutional Neural Network to remove the blur. These methods can be used in the future to improve the image quality for SfM.

4.2.2. The influence of oblique image

In this study, it was found that the average point density increased with the increase of oblique camera angle from 35° to 50° with a 5° interval, while the median of matching per calibrated image decreased. The "matching" here means that a feature point that has been detected on at least two images has been defined to be the same point. Thus, it seems like the feature points on images, which were acquired with lower oblique camera angle, are easier to be identified.

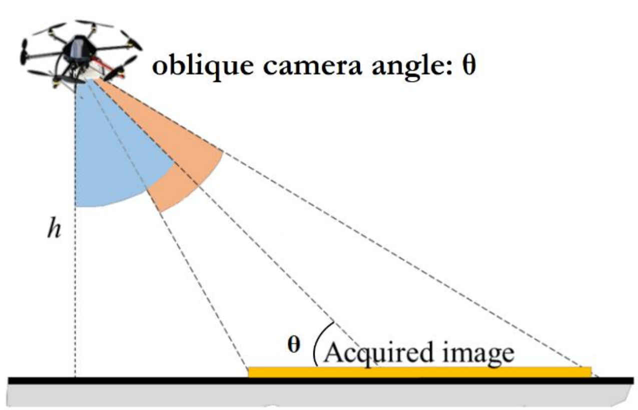

Figure 52. Camera oblique angle (Lingua et al., 2017).

Empirically, the point density should increase with the increase in matching points, because the densified point cloud is computed based on the number of matching points. However, the opposite result appeared in this study. It can be explained by the attribute of the oblique image. The resolution of the oblique image is not uniform, and the reason has been mentioned in the methodology section. The closer part of the image (to the camera) owes higher resolution, and more feature points are detected and matched (Figure 53). Assuming the flight height is constant, when the camera oblique angle decreases, the resolution decreases because the distance from the camera to object also increases. Smaller camera oblique angle will lead to poorer feature detection and matching result especially at the maximum distance from the camera to the object. Compared with the orthophoto of 50° oblique camera angle, there are more poor-quality and useless parts at a 35° oblique camera angle. It's caused by the big distance from the camera to the object at 35° camera oblique angle. Moreover, the camera with a lower oblique angle was capable of a wider view. The points were spread over a larger area, and the poor-quality and useless parts reduced the average density of the point cloud. In addition, the low texture of objects (smooth surface) resulted in low-quality feature detection and image matching in SfM (Zhang, Schneider, & Strauß, 2016), which means the point density in one image is heterogenous because of the different texture.

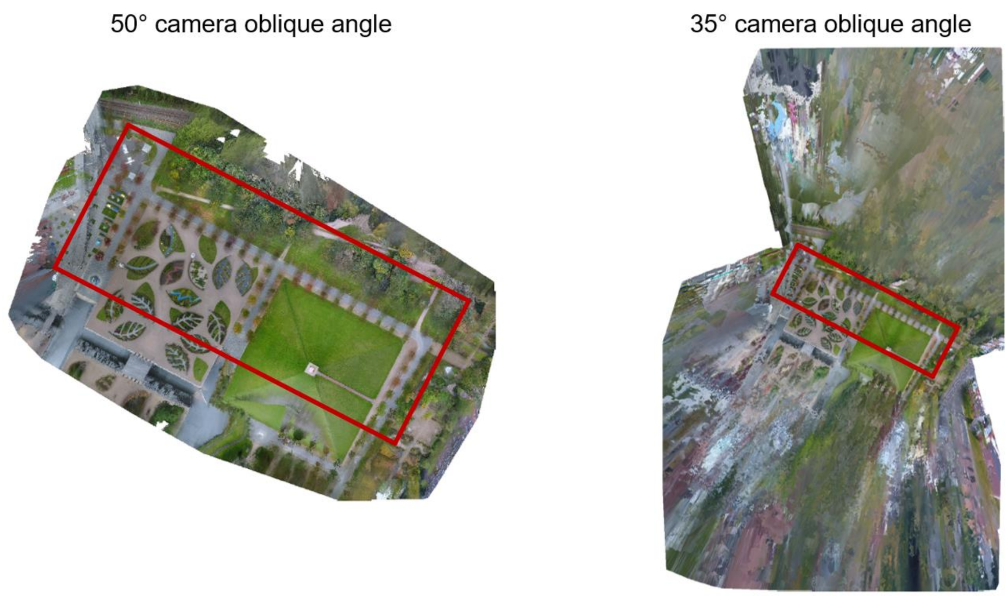

Figure 53. The orthophotos at 50° and 35° oblique camera angles. The red boundary indicates the study area.

However, the question "which angle provides the point cloud with the highest completeness" was not answered, because none of the point clouds was able to reconstruct the accurate tree structure. The poor-quality data were collected due to the bad flight condition. While during the leaf-off season, only one dataset was available because of the unreliable SD card and poor light condition, which could not be used to answer this question as well.

4.3. DBH estimation

4.3.1. DBH derived from circle fitting

There was no significant difference ($p>0.05$) between the DBH estimated by fitting a circle and the field measurements (DBH_{UAV2}&DBH_{Field}). DBH was estimated to 55.48% with an RMSE of 0.027 m during the leaf-on season, and the DBH was estimated to 52.53% with an RMSE of 0.024 m during the leaf-off season.
However, the result was obtained after removing the noise points by visual inspection, which was quite subjective. The noise points were mainly caused by the overhanging branches. Except for this, the result is in contrast with Brolly & Kiraly (2009), who observed a significant underestimation comparing the DBH estimated by fitting a circle with field measured DBH. This can be explained by the difference in input data. The UAV image-generated point cloud was similar to the first-return pulse of Lidar, while the TLS point cloud which was used in the study of Brolly & Kiraly (2009) was able to sample the rifts of the branch through the bark. The roughness of the bark depended on the tree species, which also caused the difference between the studies. Moreover, a 10-cm slice at breast height of an individual tree point cloud was used to fit the circle, and the points of the slice were projected to a horizontal plane. Thus, a leaning stem with a circular cross-section creates an elliptical projection, which would lead to overestimation (Brolly & Kiraly, 2009). Bienert, Scheller, Keane, Mullooly, & Mohan (2006) found that when only a small part of the stem was visible, the DBH would be underestimated as well. However, in this study, the bark of studied tree species was quite smooth, trees were well managed by park administration with no leaning trunk existing, and the UAV images were collected with at least two side views. The factors affected the circle fitting most in my study seemed to be the accuracy of the point cloud.

4.3.2. DBH derived from QSM

There is a significant difference ($p<0.05$) between the DBH_{Field} and the DBH estimates using QSM (DBH_{QSM} and DBH_{CYL}). The DBH_{QSM} is the diameter of the cylinder generated by the QSM at the breast height, while DBH_{CYL} is the diameter of the cylinder fitted to points at the height 1.1-1.5 m. The R^2 of DBH_{QSM}/DBH_{CYL} verse DBH_{Field} is approximately 0.4 for the leaf-on season, and more than 0.6 for the leaf-off season. The better R^2 of the leaf-off season compared with that of the leaf-on season was obtained after removing the outliers caused by incompleteness of the individual tree point cloud. The incompleteness was the result of the filtering process, QSM was prone to be inaccurate when more than 55% points of the individual tree point cloud were removed. One assumption for successful QSM reconstruction is "only sufficiently covered tree parts can be accurately reconstructed" (Raumonen, 2017). In this study, it was found that most extreme DBHs (beyond $1\pm30\%$ of DBH_{Field}) appeared when the percentage of remaining points was less than 45% for the leaf-off season. As a result, when the percentage of remaining points after filtering was less than 45%, the corresponding DBH was removed as possible outliers. After that, the R^2 increased from 0.3 to 0.6 for DBH_{QSM}/DBH_{CYL} versus DBH_{Field}, which also supported the assumption that the low completeness resulted in inaccurate tree reconstruction. Tilon (2017) also found there was a significant difference between DBH_{QSM}/DBH_{CYL} and DBH_{Field}, but she attributed this to QSM algorithm. The DBH_{QSM}/DBH_{CYL} was inaccurate if the cylinder at breast height were not well fitted with the curvatures in the stem (Tilon, 2017). Reduce the length of cylinders may improve the fitness of curvatures, but the QSM is more sensible to noise points which can easily result wrong reconstruction (Raumonen et al., 2013).
Another factor that caused an inaccurate DBH estimation was the inevitable noise in SfM (Bebis et al., 2006). The 3D point generated by SfM may show a slight deviation from the real-world position. This also occurred in other related work. Fritz et al. (2013) used a UAV image-generated point cloud to reconstruct the 3D model and estimate the tree parameter. However, noise point of SfM-cloud (red) could be observed easily in Figure

54, a good Pearson's correlation coefficient of r = 0.696 (DBH of the TLS-cloud and DBH of the SfM-cloud) was gotten with RANSAC. In the study of Fritz et al. (2013), the RANSAC based cylinder fitting was proved to be able to handle the high variation within the stem points. This algorithm can be used in the future to improve the model reconstruction.

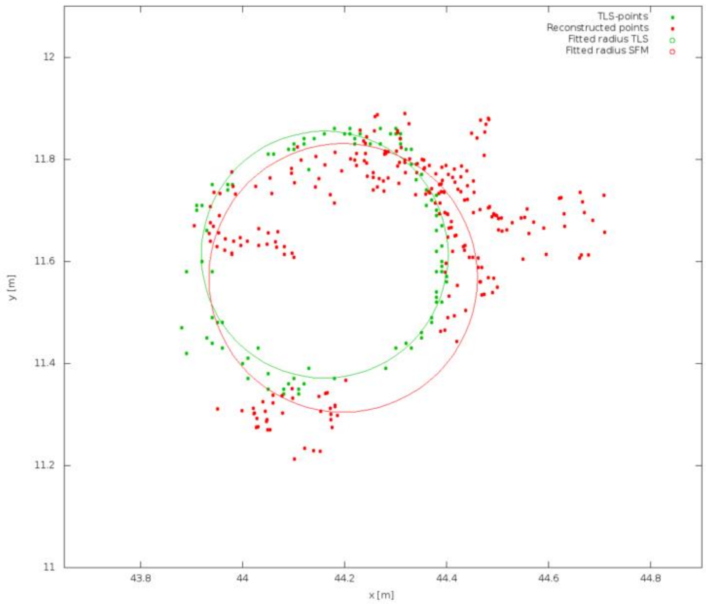

Figure 54. A 50 cm slice of a TLS stem (green) and an SfM stem (red) and their corresponding fitted diameters projected on a plane (Fritz et al., 2013).

4.3.3. DBH estimated by CPA

There was no significant difference ($p>0.05$) between the DBH estimated by CPAs and the field measurements. However, the R^2 of the regression is about 0.4, which is quite low compared with the R^2 (approximately 0.65) in the study of Shah et al. (2011). Semenzato, Cattaneo, & Dainese (2011) found that the relationship between DBH and other parameters of growth, such as leaf area and crown diameter, could not always be well predicted for unban trees. A hypothesis was that the urban trees were regularly managed with more frequent and heavier pruning. Management also happened in my case, while Shah et al. (2011) studied a natural subtropical forest without this kind of limitation. Thus, collecting the data of tree management maybe useful to verify this hypothesis.

4.4. Tree height estimation

Only $Height_{UAV}$ (the distance between the highest point and the lowest point of an individual tree point cloud) for the leaf-on season shows no significant difference compared with $Height_{Field}$. On the other hand, all estimated tree heights were well correlated with $Height_{Field}$/$Height_{ALS}$, with correlation coefficients that differed from 0.7811 to 1.0399.

The reason for the generation of a significant bias between the reference dataset and estimated dataset can be explained as follows: 1) different tools; 2) different seasons; and 3) the influence of the filtering process.

The point density of ALS data is only 1-4 points per square meters, while there are hundreds of points per cubic meter for the combined individual tree point cloud, which means more detailed information can be recorded by the UAV point cloud. In addition, as mentioned in section 4.1, the ALS pulse can penetrate the tree canopy, and this attribute will result in underestimation of tree height.

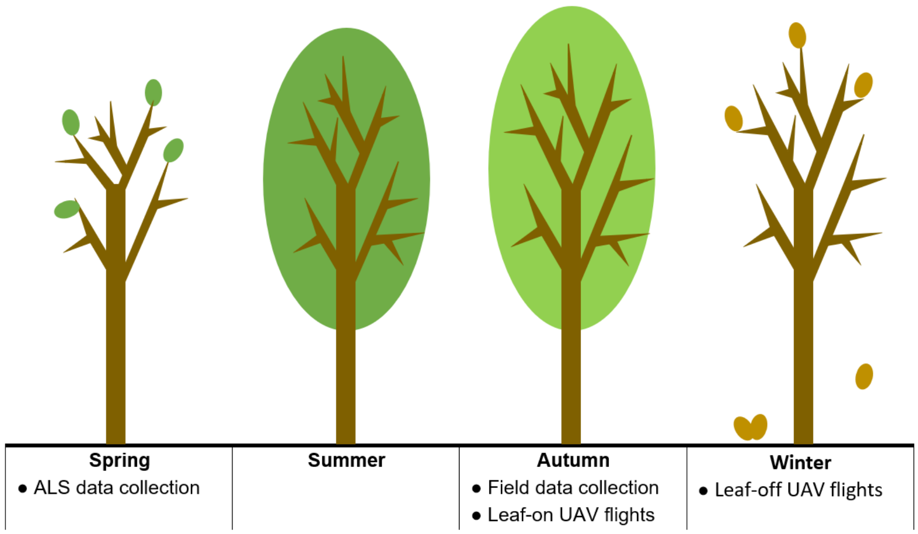

Figure 55. Field work schedule in 2017.

Figure 55 shows that $Height_{Field}$ was collected in autumn, and $Height_{ALS}$ was extracted from the ALS data collected before the growing season in early 2017. Thus, the field measured height is more up-to-date than the ALS height.

In addition, the UAV image acquisition occurred at the end of growing season as well as during the leaf-off season. Therefore, the significant difference between the datasets for the leaf-on and leaf-off seasons was reasonable.

Although there was no need to consider bias caused by the tree growing for $Height_{QSM}$ during the leaf-on season when compared with $Height_{Field}$, a significant difference was still seen between the two datasets. This is due to the filtering process which is essential for QSM. Figure 56 illustrates the influence of the filtering process; the red points defined as noise are removed, and this operation substantially reduced the tree height.

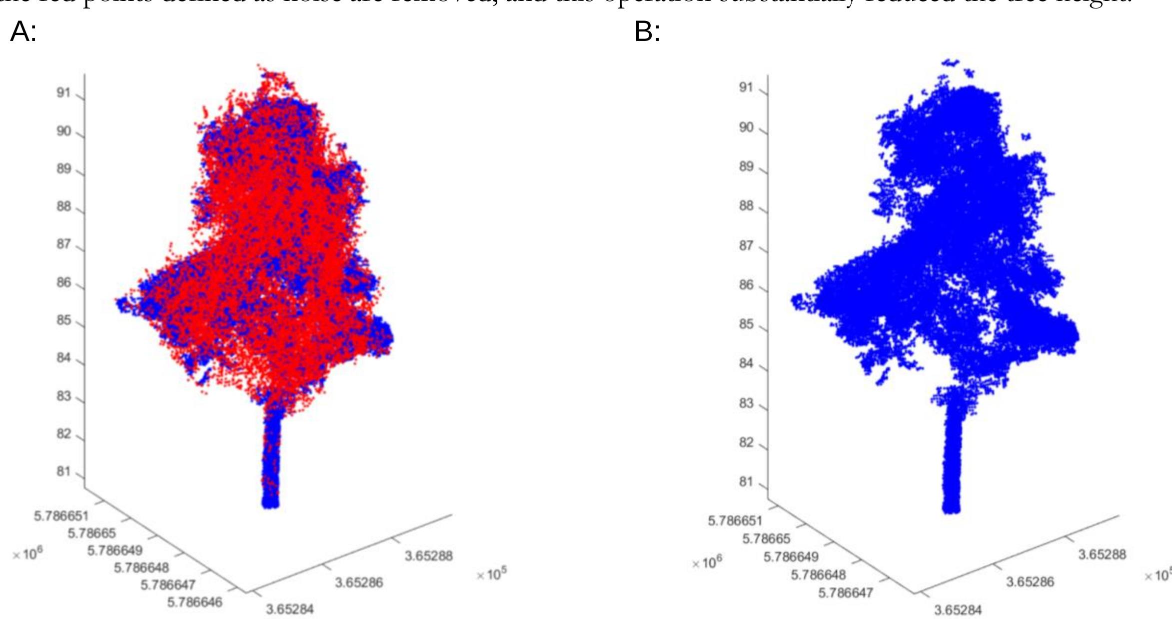

Figure 56. Filtering process. In Image A, noise points are determined and coloured in red, and Image B is the remaining point cloud after the filtering process.

4.5. Biomass estimation

There is a significant difference (p>0.05) between the QSM estimated biomass and the biomass calculated tree allometry. The biomass calculated by the QSM volume shows a 45.88% underestimation for the leaf-on season and a 43.26% underestimation for the leaf-off season. But it should be noticed that only one point cloud was used for QSM for the leaf-off season, while 4 point clouds were combined for QSM for the leaf-on season. Therefore, a better result may be generated if the same process is done for the leaf-on season.
This result is opposite to the study of Madhibha Tasiyiwa (2016). It was found that a significant difference existed when comparing AGB derived from QSM to AGB calculated by allometric equations with an overestimation of 47%. The overestimation was contributed by the bias of height estimation in a tropical forest (Madhibha Tasiyiwa, 2016). The following sections explain the possible reasons for the significant difference.

4.5.1. Uncertainty of QSM

For the leaf-on season, only trunk volume extracted from QSM can be used for the biomass calculation and assessment because the point cloud of the canopy part came from foliage and the basic assumption of QSM "the whole tree is wood" was conflicted (Raumonen, 2017). Although the canopy part was left after QSM, the biomass of the canopy was incorrectly estimated. Raumonen et al. (2011) and Krooks et al. (2014) reported that the reconstruction was poor with the presence of needles and leaves as well. In addition, the trunk biomass of QSM was still underestimated, since the trunk inside the crown was occluded by the foliage, while the allometric equation for trunk volume calculation counted the tree trunk from the base to the 5-cm top (Williams & Gresham, 2006).
For the leaf-off season, the occlusion problem caused by foliage was avoided. However, the filtering process was still necessary to eliminate the noise points produced during the SfM. Even though the number of noise points is lower, the absence of filtering leads to the wrong reconstruction (Calders et al., 2013). The trade-off of filtering intensity is important. Intensified filtering is able to remove most of the noise points, but there is a risk of removing the points that belong to the useful woody parts, less efficient filtering leaves too many noise points and will also lead to the wrong reconstruction by QSM (Madhibha Tasiyiwa, 2016).
Non-circular branches and stems result wrong QSM reconstruction as well. One assumption of QSM was that the tree surface is the cylinder (Raumonen et al., 2013), while Pfeifer, Gorte, Winterhalder, Sensing, & Range (2004) stated that the cross-sections of branch and stem were not circular in most cases.
The constant QSM parameters were another source of error. For datasets from the leaf-on and leaf-off seasons, the QSM parameters were tested using one trail tree. After that, for each dataset, the same parameters were used for the whole trees. Choosing optimal parameters for QSM is quite subjective, and the parameters might not be suitable for all trees in the dataset (Tilon, 2017).

4.5.2. Uncertainty of allometric equation

It should be considered that the studied windbreak was planted in a park and managed regularly. The management included pruning, fertilization and other preservation activities. Although the allometric equation used in this study was developed based on tree rows that were also managed, the management was carried out to eliminate the limitations of tree growth. In addition, the climate change also led to the change in stored biomass (Russell, Domke, Woodall, & D'Amato, 2015), and an unknown bias occurred when using the allometric equation developed with trees that grew in different climates. On the other hand, the allometric equation is a generic model, and a limited number of trees are used to develop the model, which reduced the range of application and predictive power (McPherson, van Doorn, & Peper, 2016). Errors in DBH, height estimates or the density measurement will result in an error in the AGB calculation (Chave et al., 2004).

5. CONCLUSION AND RECOMMENDATIONS

5.1. Conclusion

This study explored the feasibility of reconstructing QSM using UAV-derived point cloud as input data of windbreaks and individual trees. This approach is very promising in estimating above ground biomass. The research questions can be answered as followed based on the results presented in previous sections:

1. **Do camera oblique angles of UAV flights influence the point cloud density and completeness of individual tree?**

- The point density increased with the increasing of camera oblique angel. Feature points are easier to be detected and matched with a lower oblique angle.
- However, "which angle provides the point cloud with the highest completeness" was not answered due to the poor flight condition and time limitation.

2. **Is there a significant difference between the UAV point cloud derived DBH values, QSM derived DBH, CPA estimated DBH and the reference DBH?**

- There is no significant difference ($p>0.05$) between the DBH extracted form UAV-derived point cloud, DBH estimated by CPAs and reference data; while a significant difference was found between QSM-estimated DBH and the reference DBH (Leaf-on: RMSE UAV 0.027 m, RMSE QSM 0.031 m, RMSE CYL 0.032 m; Leaf-off: RMSE UAV 0.024 m, RMSE QSM 0.017 m, RMSE CYL 0.017m). It can be concluded that DBH derived from UAV point cloud using circle fitting method and DBH estimated by the regression of CPA and DBH, are accurate and can be used to estimate DBH.

3. **Is there a significant difference between the UAV point cloud derived height values, QSM derived heights and the reference heights?**

- There is no significant difference ($p>0.05$) between tree height extracted from individual tree point cloud and the height measured in the field with the Laser scanner only for the leaf-on season (RMSE 0.559 m). A significant difference exists between tree height extracted from individual tree point cloud and the height measured in the field with a laser scanner for the leaf-off season (RMSE 0.643 m).
- A significant difference exists between tree height extracted from individual tree point cloud and the height extracted from ALS data for the leaf-on and leaf-off seasons both (leaf-on RMSE 0.749 m; leaf-off RMSE 0.730 m).
- A significant difference exists between tree height estimated by QSM and the height measured in the field with laser scanner for the leaf-on and leaf-off seasons both (leaf-on RMSE 0.857 m; leaf-off RMSE 0.768 m).
- A significant difference exists between tree height estimated by QSM and the height extracted from ALS data for the leaf-on and leaf-off seasons both (leaf-on RMSE 0.993 m; leaf-off RMSE 0.902 m).
- It can be concluded that the tree height extracted from the individual tree point cloud is accurate for tree height measurement.

4. **Is there a significant difference between the AGB calculated by QSM volume, AGB calculated by allometry using DBH (estimated by CPA) and UAV-point cloud height as input, AGB calculated by point cloud derived DBH and height, AGB derived from allometry that uses QSM derived DBH and height, AGBs calculated by allometry that use reference DBH and heights as input?**

- There is a significant difference between AGB calculated by QSM volume and AGBs calculated through tree allometry for leaf-on season and leaf-off season both.
- Using the biomass calculated through allometry with field measured DBH and height as reference. The biomass estimated based on the QSM volume showed 45.88% underestimation for the leaf-on season and 43.26% underestimation for the leaf-off season. The biomass calculated through allometry with QSM-derived DBH and tree height showed 31.62% underestimation for the leaf-on season and 17.09% underestimation for the leaf-off season. Besides, four point clouds were combined for QSM for the leaf-on season, while only one point cloud was used for the leaf-off season. It can be concluded that the QSM behaved better during the leaf-off season with UAV-generated point cloud as input.

5.2. Recommendations

- Prepare the UAV flights considering the weather condition, reliability of equipment.
- Collect UAV data during the leaf-off season.
- Use RANSAC for fitting a circle to handle the high variation of points at breast height.
- Validate the accuracy of QSM biomass through destructive sampling.

LIST OF REFERENCES

A.Burt, M.I.Disney, P.Raumonen, J.Armston, And, K. C., & P.Lewis. (2013). Rapid characterisation of forest structure from TLS and 3D modelling. *IGARSS*, (128.197.168.195[PDF]), 3387–3390. https://doi.org/10.1109/IGARSS.2013.6723555

Aicardi, I., Dabove, P., Lingua, A. M., & Piras, M. (2017). Integration between TLS and UAV photogrammetry techniques for forestry applications. *IForest*, *10*(1), 41–47. https://doi.org/10.3832/ifor1780-009

Antonarakis, A., Saatchi, S. S., Chazdon, R. L., & Moorcroft, P. R. (2011). Using Lidar and Radar measurements to constrain predictions of forest ecosystem structure and function. *Ecological Applications*, *21*(4), 1120–1137. https://doi.org/10.1890/10-0274.1

Bebis, G., Boyle, R., Parvin, B., Koracin, D., Remagnino, P., Nefian, A., … Malzbender, T. (2006). *Advances in Visual Computing, Second International Symposium, ISVC 2006 Lake Tahoe, NV, USA, November 6-8, 2006. Proceedings, Part I.*

Bernasconi, L., Chirici, G., & Marchetti, M. (2017). Biomass estimation of xerophytic forests using visible aerial imagery: Contrasting single-tree and area-based approaches. *Remote Sensing*, *9*(4), 1–12. https://doi.org/10.3390/rs9040334

Bezirksregierung Köln. (2016a). Digitale Geländemodelle (DGM). Retrieved August 22, 2017, from http://www.bezreg-koeln.nrw.de/brk_internet/geobasis/hoehenmodelle/gelaendemodelle/index.html

Bezirksregierung Köln. (2016b). Digitales Oberflächenmodell (DOM). Retrieved August 22, 2017, from http://www.bezreg-koeln.nrw.de/brk_internet/geobasis/hoehenmodelle/oberflaechenmodell/index.html

Bienert, A., Scheller, S., Keane, E., Mullooly, G., & Mohan, F. (2006). Application of Terrestrial Laser Scanners For The Determination Of Forest Inventory Parameters. *International Archives of Photogrammetry , Remote Sensing and Spatial Information Science*, *36*, 5. https://doi.org/10.1111/jam.12647

Brolly, G., & Kiraly, G. (2009). Algorithms for stem mapping by means of terrestrial laser scanning. *Acta Silvatica et Lignaria Hungarica*, *5*, 119–130. Retrieved from http://search.ebscohost.com/login.aspx?direct=true&profile=ehost&scope=site&authtype=crawler&jrnl=1787064X&AN=48132484&h=JFuiyfYfJjT3Nwxv6gvqBkJ09T/OXgadcKYbuk+wcr0VWU9tWRh2ZSXuttEBPmqSztewqWU2ZhVE2iuS49WihA==&crl=c

Brown, S. (2002). Measuring carbon in forests: Current status and future challenges. *Environmental Pollution*, *116*(3), 363–372. https://doi.org/10.1016/S0269-7491(01)00212-3

Calders, K., Newnham, G. J., Herold, M., Murphy, S., Culvenor, D. S., Raumonen, P., … Disney, M. I. (2013). *Estimating above ground biomass from terrestrial laser scanning in Australian Eucalypt Open Forest. Proceedings of SilviLaser 2013* (Vol. di).

Chave, J., Andalo, C., Brown, S., Cairns, M. A., Chambers, J. Q., Eamus, D., … Yamakura, T. (2005). Tree allometry and improved estimation of carbon stocks and balance in tropical forests. *Oecologia*, *145*(1), 87–99. https://doi.org/10.1007/s00442-005-0100-x

Chave, J., Condit, R., Aguilar, S., Hernandez, A., Lao, S., & Perez, R. (2004). Error propagation and scaling for tropical forest biomass estimates. *Philosophical Transactions of the Royal Society B: Biological Sciences*, *359*(1443), 409–420. https://doi.org/10.1098/rstb.2003.1425

Dassot, M., Constant, T., & Fournier, M. (2011). The use of terrestrial LiDAR technology in forest science: Application fields, benefits and challenges. *Annals of Forest Science*, *68*(5), 959–974. https://doi.org/10.1007/s13595-011-0102-2

Dittmann, S., Thiessen, E., & Hartung, E. (2017). Applicability of different non-invasive methods for tree mass estimation: A review. *Forest Ecology and Management*, *398*, 208–215. https://doi.org/10.1016/j.foreco.2017.05.013

Falkowski, M. J., Smith, A. M. S., Gessler, P. E., Hudak, A. T., Vierling, L. A., & Evans, J. S. (2008). The influence of conifer forest canopy cover on the accuracy of two individual tree measurement algorithms using lidar data. *Canadian Journal of Remote Sensing*, *34*(Supplement 2), 338–350. https://doi.org/10.5589/m08-055

Fritz, A., Kattenborn, T., & Koch, B. (2013). UAV-based photogrammetric point clouds- tree stem mapping

in open stands in comparison to Terrestrial Laser Scanner point clouds. *ISPRS - International Archives of the Photogrammetry, Remote Sensing and Spatial Information Sciences*, *XL-1/W2*(September), 141–146. https://doi.org/10.5194/isprsarchives-XL-1-W2-141-2013
Gill, S. J., Biging, G. S., & Murphy, E. C. (2000). Modeling conifer tree crown radius and esimating canopy cover. *Forest Ecology and Management*, *126*, 405–416.
Gonzalez de Tanago Menaca, J., Lau, A., Bartholomeusm, H., Herold, M., Avitabile, V., Raumonen, P., … Calders, K. (2017). Estimation of above-ground biomass of large tropical trees with Terrestrial LiDAR. *Methods in Ecology and Evolution*, *2017*(July), 1–12. https://doi.org/10.1111/2041-210X.12904
Henning, J. G., & Radtke, P. J. (2006). Detailed stem measurements of standing trees from ground-based scanning lidar. *Forest Science*, *52*(1), 67–80.
Hopkinson, C., Chasmer, L., Young-Pow, C., & Treitz, P. (2004). Assessing forest metrics with a ground-based scanning lidar. *Canadian Journal of Forest Research*, *34*(3), 573–583. https://doi.org/10.1139/x03-225
Houghton, R. A. (2005). Aboveground forest biomass and the global carbon balance. *Global Change Biology*, *11*(6), 945–958. https://doi.org/10.1111/j.1365-2486.2005.00955.x
Johnson, R. L. (1985). Sweetgum, an American Wood. *FS-266. Washington, DC: US Department of Agriculture, Forest Service.*
Kirby, K. R., & Potvin, C. (2007). Variation in carbon storage among tree species: Implications for the management of a small-scale carbon sink project. *Forest Ecology and Management*, *246*(2–3), 208–221. https://doi.org/10.1016/j.foreco.2007.03.072
Köhl, M., Magnussen, S., & Marchetti, M. (2006). *Sampling Methods, Remote Sensing and GIS Multiresource Forest Inventory. Springer-Verlag Berlin Heidelberg New York* (Vol. 3). https://doi.org/10.1300/J091v03n02_06
Krooks, A., Kaasalainen, S., Kankare, V., Joensuu, M., Raumonen, P., & Kaasalainen, M. (2014). Predicting tree structure from tree height using terrestrial laser scanning and quantitative structure models. *Silva Fennica*, *48*(2), 1–11. https://doi.org/10.14214/sf.1125
Lee, H. S., & Lee, K. M. (2013). Dense 3D reconstruction from severely blurred images using a single moving camera. *Proceedings of the IEEE Computer Society Conference on Computer Vision and Pattern Recognition*, 273–280. https://doi.org/10.1109/CVPR.2013.42
Lin, Y., Jiang, M., Yao, Y., Zhang, L., & Lin, J. (2015). Use of UAV oblique imaging for the detection of individual trees in residential environments. *Urban Forestry and Urban Greening*, *14*(2), 404–412. https://doi.org/10.1016/j.ufug.2015.03.003
Lingua, A., Noardo, F., Spanò, A. T., Sanna, S., & Matrone, F. (2017). 3D Model Generation Using Oblique Images Acquired By Uav. *ISPRS - International Archives of the Photogrammetry, Remote Sensing and Spatial Information Sciences*, *XLII-4/W2*(July), 107–115. https://doi.org/10.5194/isprs-archives-XLII-4-W2-107-2017
Liu, J., Guo, B., Jiang, W., Gong, W., & Xiao, X. (2016). Epipolar rectification with minimum perspective distortion for oblique images. *Sensors (Switzerland)*, *16*(11), 1–17. https://doi.org/10.3390/s16111870
Mader, D., Blaskow, R., Westfeld, P., & Maas, H. G. (2015). UAV-Based acquisition of 3D point cloud - A comparison of a low-cost laser scanner and SFM-tools. *International Archives of the Photogrammetry, Remote Sensing and Spatial Information Sciences - ISPRS Archives*, *40*(3W3), 335–341. https://doi.org/10.5194/isprsarchives-XL-3-W3-335-2015
Madhibha Tasiyiwa, P. (2016). *Assessment of above ground biomass with terrestrial LIDAR using 3D Quantitative Structure Modelling in Tropical Rain Forest of Ayer Hitam Forest Reserve, Malaysia*. University of Twente. Retrieved from http://www.itc.nl/library/papers_2016/msc/nrm/madhibha.pdf
Mancini, F., Dubbini, M., Gattelli, M., Stecchi, F., Fabbri, S., & Gabbianelli, G. (2013). Using unmanned aerial vehicles (UAV) for high-resolution reconstruction of topography: The structure from motion approach on coastal environments. *Remote Sensing*, *5*(12), 6880–6898. https://doi.org/10.3390/rs5126880
McPherson, E. G., van Doorn, N., & Peper, P. (2016). *Urban Tree Database and Allometric Equations*. https://doi.org/10.13140/RG.2.2.35769.98405
Mehtätalo, L., Virolainen, A., Tuomela, J., & Packalen, P. (2015). Estimating Tree Height Distribution Using Low-Density ALS DataWith and Without Training Data. *IEEE Journal of Selected Topics in Applied Earth*

Observations and Remote Sensing, *8*(4), 1432–1441.
Miller, J., Morgenroth, J., & Gomez, C. (2015). 3D modelling of individual trees using a handheld camera: Accuracy of height, diameter and volume estimates. *Urban Forestry and Urban Greening*, *14*(4), 932–940. https://doi.org/10.1016/j.ufug.2015.09.001
Morgenroth, J., & Gomez, C. (2014). Assessment of tree structure using a 3D image analysis technique-A proof of concept. *Urban Forestry and Urban Greening*, *13*(1), 198–203. https://doi.org/10.1016/j.ufug.2013.10.005
Næsset, E., & Gobakken, T. (2008). Estimation of above- and below-ground biomass across regions of the boreal forest zone using airborne laser. *Remote Sensing of Environment*, *112*(6), 3079–3090. https://doi.org/10.1016/j.rse.2008.03.004
Nair, P. K. R., Kumar, B. M., & Nair, V. D. (2009). Agroforestry as a strategy for carbon sequestration. *Journal of Plant Nutrition and Soil Science*, *172*(1), 10–23. https://doi.org/10.1002/jpln.200800030
Nex, F. (2017). *UAV FOR EARTH OBSERVATION STRUCTURE FROM MOTION - SFM: Powerpoint slides*. Retrieved from blackboard.utwente.nl/bbcswebdav/pid-1059942-dt-content-rid-2617656_2/courses/M17-EOS-104/04_SfM.pdf
Nowak, D. J., Greenfield, E. J., Hoehn, R. E., & Lapoint, E. (2013). Carbon storage and sequestration by trees in urban and community areas of the United States. *Environmental Pollution*, *178*, 229–236. https://doi.org/10.1016/j.envpol.2013.03.019
Paul Schmid-Haas, Ernst Baumann, J. W. (1978). *Kontrollstichproben: Aufnahmeinstruktion* (2nd edn). Eidg. Anstalt für das Forstliche Versuchswesenth. Retrieved from https://books.google.nl/books/about/Kontrollstichproben.html?id=0S9SHAAACAAJ&redir_esc=y
Pfeifer, N., Gorte, B., Winterhalder, D., Sensing, R., & Range, C. (2004). Automatic Reconstruction of Single Trees from Terrestrial Laser Scanner Data. *ISPRS - International Archives of the Photogrammetry, Remote Sensing and Spatial Information Sciences*, *XXXV*(5), 114–119. https://doi.org/10.1111/jam.12647
Philip Rowe. (2007). *Essential Statistics for the Pharmaceutical Sciences*. Hoboken: John Wiley and Sons Ltd. Retrieved from https://www.bookdepository.com/Essential-Statistics-for-Pharmaceutical-Sciences-Philip-Rowe/9780470034705
Pollefeys, M., Van Gool, L., Vergauwen, M., Verbiest, F., Cornelis, K., Tops, J., & Koch, R. (2004). Visual modeling with a hand-held camera. *International Journal of Computer Vision*, *59*(3), 207–232. https://doi.org/10.1023/B:VISI.0000025798.50602.3a
Rango, A., Laliberte, A. S., & Havstad, K. M. (2014). Unmanned aerial vehicle-based remote sensing for rangeland assessment , monitoring , and management, (August 2009). https://doi.org/10.1117/1.3216822
Raumonen, P. (2017). *TreeQSM Quantitative Structure Models of Single: Instructions for MATLAB-software TreeQSM, version 2.30*. Retrieved from https://github.com/InverseTampere/TreeQSM/tree/master/Manual
Raumonen, P., Kaasalainen, M., Åkerblom, M., Kaasalainen, S., Kaartinen, H., Vastaranta, M., … Lewis, P. (2013). Fast Automatic Precision Tree Models from Terrestrial Laser Scanner Data. *Remote Sensing*, *5*(2), 491–520. https://doi.org/10.3390/rs5020491
Raumonen, P., Kaasalainen, S., Kaasalainen, M., & Kaartinen, H. (2011). Approximation of Volume and Branch Size Distribution of Trees From Laser Scanner Data. *ISPRS - International Archives of the Photogrammetry, Remote Sensing and Spatial Information Sciences*, *XXXVIII-5*(W12), 79–84. https://doi.org/10.5194/isprsarchives-XXXVIII-5-W12-79-2011
Richard Brown. (2007). fitcircle.m. *Matlab Central File Exchange*. Retrieved from https://nl.mathworks.com/matlabcentral/fileexchange/15060-fitcircle-m
Richard Hartley, A. Z. (2003). *Multiple View Geometry in Computer Vision*. *Cambridge University Press*. Cambridge. https://doi.org/10.1017/CBO9781107415324.004
Rosnell, T., & Honkavaara, E. (2012). Point cloud generation from aerial image data acquired by a quadrocopter type micro unmanned aerial vehicle and a digital still camera. *Sensors*, *12*(1), 453–480. https://doi.org/10.3390/s120100453
Ruiz, L. A., Hermosilla, T., Mauro, F., & Godino, M. (2014). Analysis of the influence of plot size and LiDAR density on forest structure attribute estimates. *Forests*, *5*(5), 936–951. https://doi.org/10.3390/f5050936

Russell, M. B., Domke, G. M., Woodall, C. W., & D'Amato, A. W. (2015). Comparisons of allometric and climate-derived estimates of tree coarse root carbon stocks in forests of the United States. *Carbon Balance and Management*, *10*(1). https://doi.org/10.1186/s13021-015-0032-7

Schoeneberger, M. M. (2009). Agroforestry: Working trees for sequestering carbon on agricultural lands. *Agroforestry Systems*, *75*(1), 27–37. https://doi.org/10.1007/s10457-008-9123-8

Semenzato, P., Cattaneo, D., & Dainese, M. (2011). Growth prediction for five tree species in an Italian urban forest. *Urban Forestry and Urban Greening*, *10*(3), 169–176. https://doi.org/10.1016/j.ufug.2011.05.001

Shah, S. K., Hussin, Y. A., Leeuwen, L. M. van, & Gilani, H. (2011). Modelling the relationship between tree canopy projection area and above ground carbon stock using high resolution geoeye satellite images. *ACRS 2011 : Proceedings of the 32nd Asian Conference on Remote Sensing : Sensing for Green Asia, 3-7 October 2011, Taipei, Taiwan*, 6.

Shahbazi, M., Sohn, G., Théau, J., & Menard, P. (2015). Development and Evaluation of a UAV-Photogrammetry System for Precise 3D Environmental Modeling, 27493–27524. https://doi.org/10.3390/s151127493

Shimano, K. (1997). Analysis of the relationship between DBH and crown projection area using a new model. *Journal of Forest Research*, *2*(4), 237–242. https://doi.org/10.1007/BF02348322

Sieberth, T., Wackrow, R., & Chandler, J. H. (2014). Influence of blur on feature matching and a geometric approach for photogrammetric deblurring. *International Archives of the Photogrammetry, Remote Sensing and Spatial Information Sciences - ISPRS Archives*, *40*(3), 321–326. https://doi.org/10.5194/isprsarchives-XL-3-321-2014

Sieberth, T., Wackrow, R., & Chandler, J. H. (2015). UAV image blur-its influence and ways to correct it. *International Archives of the Photogrammetry, Remote Sensing and Spatial Information Sciences - ISPRS Archives*, *40*(1W4), 33–39. https://doi.org/10.5194/isprsarchives-XL-1-W4-33-2015

Stem volume. (2013). Retrieved January 16, 2018, from http://wiki.awf.forst.uni-goettingen.de/wiki/index.php/Stem_volume

Suárez, J. C., Ontiveros, C., Smith, S., & Snape, S. (2005). Use of airborne LiDAR and aerial photography in the estimation of individual tree heights in forestry. *Computers and Geosciences*, *31*(2), 253–262. https://doi.org/10.1016/j.cageo.2004.09.015

Sun, J., Cao, W., Xu, Z., & Ponce, J. (2015). Learning a convolutional neural network for non-uniform motion blur removal. *Proceedings of the IEEE Computer Society Conference on Computer Vision and Pattern Recognition*, *07–12–June*, 769–777. https://doi.org/10.1109/CVPR.2015.7298677

Tansey, K., Selmes, N., Anstee, A., Tate, N. J., & Denniss, A. (2009). Estimating tree and stand variables in a Corsican Pine woodland from terrestrial laser scanner data. *International Journal of Remote Sensing*, *30*(19), 5195–5209. https://doi.org/10.1080/01431160902882587

Tilon, S. M. (2017). *The effect of foliage on estimating above ground forest biomass using Terrestrial Laser Scanning and Quantitative Structure Modelling in Gronau, Germany*. University of Twente.

Udawatta, R. P., & Jose, S. (2012). Agroforestry strategies to sequester carbon in temperate North America. *Agroforestry Systems*, *86*(2), 225–242. https://doi.org/10.1007/s10457-012-9561-1

Westoby, M. J., Brasington, J., Glasser, N. F., Hambrey, M. J., & Reynolds, J. M. (2012). *"Structure-from-Motion" photogrammetry: A low-cost, effective tool for geoscience applications*. *Geomorphology* (Vol. 179). Elsevier B.V. https://doi.org/10.1016/j.geomorph.2012.08.021

Wierzbicki, D., Kedzierski, M., & Fryskowska, A. (2015). Assesment of the influence of UAV image quality on the orthophoto production. *International Archives of the Photogrammetry, Remote Sensing and Spatial Information Sciences - ISPRS Archives*, *40*(1W4), 1–8. https://doi.org/10.5194/isprsarchives-XL-1-W4-1-2015

Williams, T. M., & Gresham, C. A. (2006). Biomass accumulation in rapidly growing loblolly pine and sweetgum. *Biomass and Bioenergy*, *30*(4), 370–377. https://doi.org/10.1016/j.biombioe.2005.07.017

Xiao, Q., & McPherson, G. G. (2011). Rainfall interception of three trees in Oakland, California. *Urban Ecosystems*, *14*(4), 755–769. https://doi.org/10.1007/s11252-011-0192-5

Zanne, A. E., Lopez-Gonzalez, G., Coomes, D. A., Ilic, J., Jansen, S., Lewis, S. L., … Chave, J. (2009). Data from: Towards a worldwide wood economics spectrum. *Ecology Letters*. Dryad Digital Repository. https://doi.org/doi:10.5061/dryad.234

Zarco-Tejada, P. J., Diaz-Varela, R., Angileri, V., & Loudjani, P. (2014). Tree height quantification using very high resolution imagery acquired from an unmanned aerial vehicle (UAV) and automatic 3D photo-reconstruction methods. *European Journal of Agronomy*, *55*, 89–99. https://doi.org/10.1016/j.eja.2014.01.004

Zhang, R., Schneider, D., & Strauß, B. (2016). Generation and comparison of TLs and SFM based 3D models of solid shapes in hydromechanic research. *International Archives of the Photogrammetry, Remote Sensing and Spatial Information Sciences - ISPRS Archives*, *41*(July), 925–929. https://doi.org/10.5194/isprsarchives-XLI-B5-925-2016

ANNEX

	A	B	C	D	E	F	G
1	Tree ID	All points	Points left	Percentage	DBH_Field	DBH_QSM	DBH_CYL
26	25	44903	29470	65.63	0.185	0.147	0.150
27	26	227543	134165	58.96	0.270	0.224	0.228
28	27	85735	42427	49.49	0.245	0.217	0.210
29	28	117204	62837	53.61	0.254	0.227	0.234
30	29	123699	66402	53.68	0.236	0.119	0.119
31	30	114927	68536	59.63	0.250	0.199	0.209
32	31	24449	16527	67.60	0.115	0.122	0.125
33	32	26966	10850	40.24	0.134	0.097	0.097
34	33	6442	363	5.63	0.205	0.174	0.174
35	37	13029	3653	28.04	0.186	0.037	0.037
36	38	14532	3425	23.57	0.210	0.070	0.070
37	40	33184	4788	14.43	0.200	0.049	0.049
38	41	19516	7212	36.95	0.216	0.149	0.143
39	42	39960	19869	49.72	0.205	0.200	0.200
40	43	26285	16433	62.52	0.161	0.165	0.164
41	44	49105	33733	68.70	0.208	0.190	0.197
42	45	48035	31616	65.82	0.205	0.190	0.197
43	46	75175	50751	67.51	0.190	0.157	0.162
44	47	59849	42873	71.64	0.220	0.190	0.196
45	48	69019	49098	71.14	0.209	0.166	0.168
46	49	97305	63770	65.54	0.232	0.213	0.205
47	50	127248	74047	58.19	0.180	0.168	0.172

Annex Figure 1. The screenshot of checking extreme DBHs in excel. The QSM estimated DBH of highlighted trees are much smaller than the reference DBH.